INL-RPT-21-66031
Revision 0

Concurrent Cooling Effects of Dynamic Line Ratings on Wind Plant Gen-Tie Lines

March 2022

Alexander Abboud
Jacob Lehmer
Jake Gentle

Changing the World's Energy Future

Idaho National Laboratory

INL is a U.S. Department of Energy National Laboratory operated by Battelle Energy Alliance, LLC

INL-RPT-21-66031
Revision 0

Concurrent Cooling Effects of Dynamic Line Ratings on Wind Plant Gen-Tie Lines

Alexander Abboud
Jacob Lehmer
Jake Gentle

March 2022

Idaho National Laboratory
Idaho Falls, Idaho 83415

http://www.inl.gov

Prepared for the
U.S. Department of Energy
Wind Energy Technologies Office
Under DOE Idaho Operations Office
Contract DE-AC07-05ID14517

Page intentionally left blank

SUMMARY

This report was prepared for the Wind Energy Technology Office for the FY 2022, quarter 2 deliverable. This details the use of dynamic line rating technology to rate a series of gen tie lines connecting wind plants to the regional transmission lines. This consists of two primary study regions, the first on the desert west of Idaho Falls, and the second in the region east of the Cascades along the Columbia River Gorge. The TREAD program that was developed at INL was used to create generated gen-tie lines based on nearby regional transmission line connections. The capacity availability of the gen tie lines are compared with the power production of the wind farms. Overall, the INL Site location shows a much greater capacity for the gen-tie lines due to the higher wind speeds. Across both locations, the HRRR data shows higher wind speeds than observed at the observational weather stations. For both the Columbia Gorge and Idaho areas, many of the sites show that a statically rate gen-tie could carry additional capacity far above the rated during periods of high wind due to the concurrent cooling effects.

Page intentionally left blank

CONTENTS

FIGURES

TABLES

Page intentionally left blank

ACRONYMS

CFD	Computational Fluid Dynamics
DLR	Dynamic Line Rating
GLASS	General Line Ampacity State Solver
RANS	Reynolds-averaged Navier-Stokes
TREAD	Transmission Route Engineering Analysis and Design

Page intentionally left blank

Dynamic Line Rating Study of Concurrent Cooling for a Proposed Wind Farm

1. Introduction

Transmission line ratings are given by a maximum ampacity based on the maximum conductor temperature limits, which are typically set to avoid sagging or clearance issues of the transmission line segments between structures due to thermal expansion. The dependency of maximum ampacity on the maximum temperature and weather conditions has standard models that were developed by the International Council on Large Electric Systems (CIGRE) (CIGRE 1992; CIGRE 2006; CIGRE 2014), the International Electrochemical Commission (IEC) (IEC 1985) and the Institute of Electrical and Electronics Engineers (IEEE) (IEEE 2012; IEEE 2016).

The weather conditions used in these methods are typically constant values year-round or with seasonal patterns, and are set using conservative assumptions for the conditions. By not accounting for additional cooling during periods of high wind or low ambient temperature, there is likely unused head room on many overhead transmission lines. Dynamic Line Rating (DLR) uses a changing line rating based on local conditions rather than a static rating assumption to provide additional ampacity capacity to a transmission line. DLR has been identified by the United States Department of Energy as a distribution infrastructure solution to defer upgrades, support line outages, and increase yields of distributed generation (US DOE, 2010; US DOE 2014).

The conservative nature of transmission line standards and the regional transmission operators (RTOs) can be hard to adjust, so research showing the benefits of DLR is important to prove the benefits of the method. Case studies utilizing weather data in the field has shown potential for DLR to increase ampacity above static throughout several countries (Greenwood et al., 2014; Bhattarai et al., 2017; Bhattarai et al., 2018; Usik-Joustenvuo and Pasonen, 2013; Aznarte and Siebert, 2017) Further studies have involved coupling the weather data with forecast model to be used for forecasted ratings, and assessment of risk (Abboud et al., 2019b).

This study utilizes the coupling of field weather data and weather model data from the High-resolution rapid refresh model (HRRR) within the region of interest with Computational Fluid Dynamics (CFD) results. For the wind field simulations, the steady-state Reynolds-Averaged Navier Stokes (RANS) approach was used for turbulent modelling of the wind flow (Jones and Launder, 1972). The RANS approach has been used to validate wind flows in complex terrains (Wallbank, 2008) with adequate speed up predictions (Dhunny et al., 2016) and low-elevation mountains within acceptable error (Dhunny et al., 2015; Dhunny et al., 2017). Due to the convective cooling calculation, the error in the cooling rate scales as approximate the square root of the wind speed, so a 10% error in wind speed is only a 5% error in the cooling rate. The site of interest in just outside of the Idaho National Laboratory property boundary in eastern Idaho, with a domain extent of 40 km by 40 km.

The weather forecasts used in this study came from version 3 of the HRRR model. HRRR is a convection-allowing forecast model that outputs meteorological variables on a 3-km horizontal grid over the continental United States (Benjamin et al., 2016; Smith et al., 2008).The HRRR was developed at the National Oceanic and Atmospheric Administration (NOAA) Earth System Research Laboratory and is run operationally at the National Center for Environmental Prediction (NCEP). The previous version of the HRRR, Version 3, became operational on 12 July 2018 and outputs forecasts from zero through 18 hours with 15-minute temporal resolution that are updated every hour. The model also outputs forecasts from zero to 36 hours with one-hour temporal resolution at 00, 06, 12, and 18 UTC. While the HRRR version 4 recently became operational and allows for 48 hour forecasts, this was only in December 2020, so not enough data is available yet.

In addition to transmission lines for regional power, another benefit to DLR is concurrent cooling effects associated with wind farms. With higher wind speeds, the power generation of wind farms increases at the same time that the ampacity of a transmission line is increased due to higher cooling rates. This effect could be used to avoid curtailment of power generation, and some studies have proved this correlation (Cao et al., 2016; Talpur et al., 2015, Banerjee et al., 2015). Here, we seek to expand the research by looking at the rating of a transmission line prior to the construction to select a proper conductor with DLR in mind. Figure 1a shows the region of interest of the proposed wind farm. This map contains the rows of turbines marked with the flags along with the lettering/numbering of each. The two push pins denote the approximate locations of the collector substations. The proposed gen tie line would run parallel to highway 20 in the map. In the CFD model, the underperforming wind turbines are cut out of this initial plan, and only the most efficient turbines are utilized. Figure 1b shows the region of interest along the Columbia River Gorge https://bpagis.maps.arcgis.com/apps/webappviewer/index.html?id=275cd78c003349719b28f7130d4b933e

https://bpagis.maps.arcgis.com/apps/webappviewer/index.html?id=43e1c8ed8ad44e4b8890d2e870b591b4. The green locations are taken as the approximate center of the wind plants to model, and the pink lines show the regional transmission to connect to via gen-tie lines.

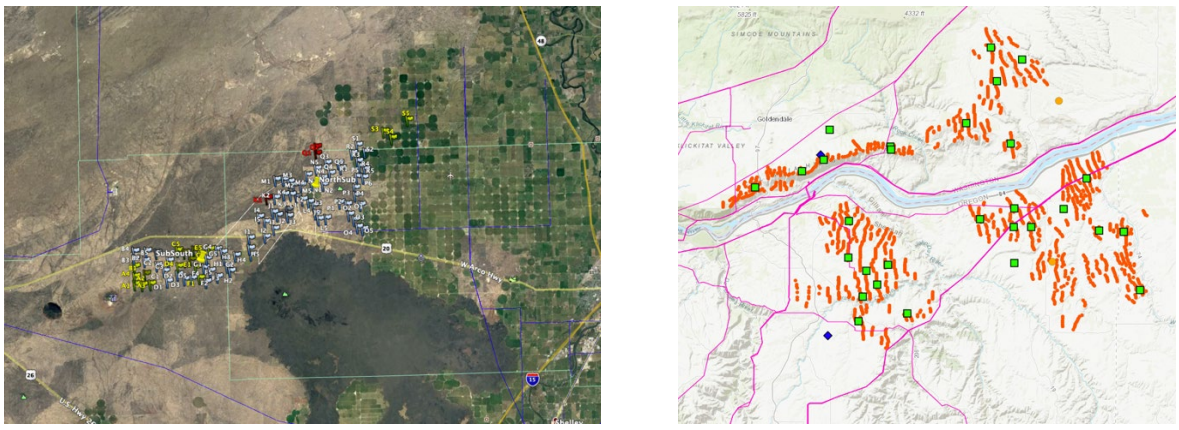

(a) (b)

Figure 1. The region of interest for the (a) INL site wind farm and (b) Columbia River Gorge wind farms

2. Study Regions

2.1 INL Desert

The CFD domain is set up as shown in Figure 2. Figure 2a shows the elevation map with the wind turbine locations, 2b shows the roughness layer, 2c shows gen-tie line 1, and 2d shows gen tie-line 2. The elevation map scale is in meters showing low areas and green, and high areas, such as nearby buttes in brown. The roughness layer shows regions of low to high vegetation and cities where near ground wind fields would be affected. These regions are not explicitly modelled in the CFD, so the roughness layer is used to approximate slowdowns due to these subgrid effects. This value is set to 1.0 for city regions (dark red on the scale), 0.8 for heavily forested areas (red on the scale), 0.1 - 0.2 for farmland or plains covered in shrubs (yellow on the scale), and set to 0 (white on the scale) for flat areas, such as along the water surface, and for areas with very little vegetation. The roughness values are used in the log- law correlations for the boundary layer with values adapted from Troen and Petersen, 1989. This wind farm is set up for a total of 78 turbine locations with a total output of 450 MW. The first gen tie line runs from the collector for the southwestern turbines up to the collector for the northeastern cluster of turbines. It is

assumed that the total power output is split in half such that this line carries a maximum 225MW. The second gen tie line runs from this northeastern collector along the highway out to the main regional transmission lines. The end point is at a transformer station along the regional transmission lines which already exists.

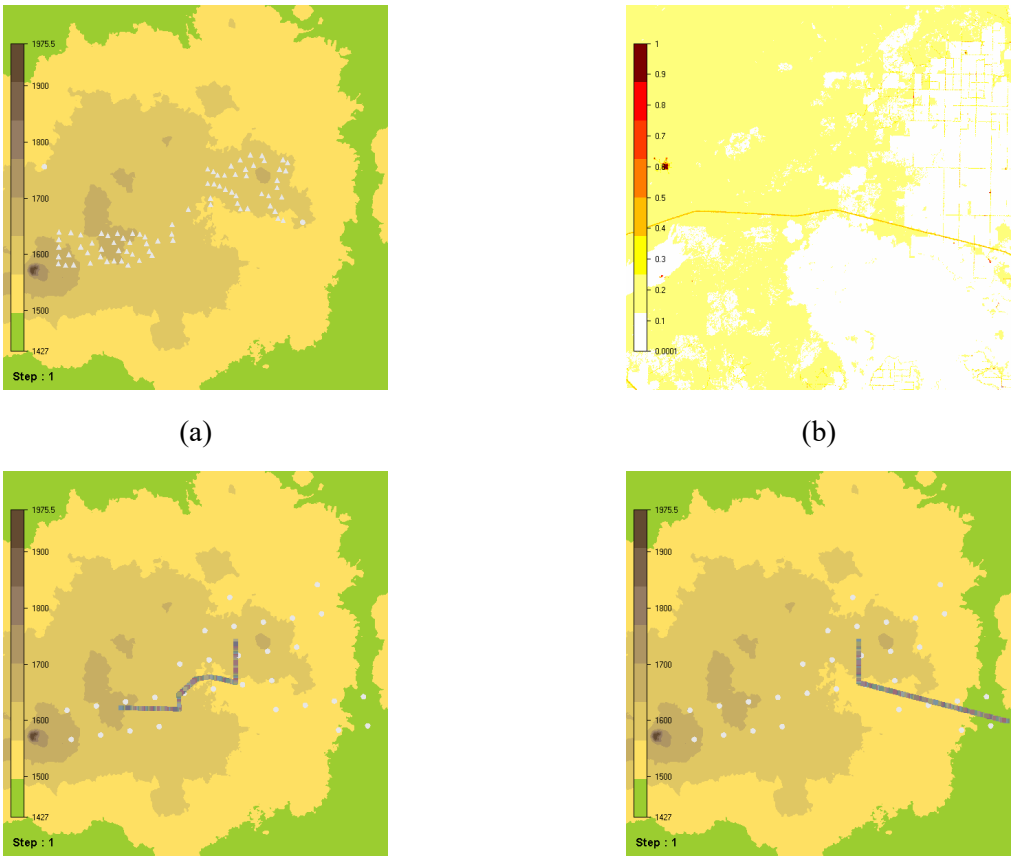

(a) (b)

(c) (d)

Figure 2. The region of interest for the wind farm with (a) wind turbine layout, (b) roughness layer, (c) gen tie line 1 and (d) gen tie-line 2.

The turbines at the proposed wind farm are assumed to be Siemen-Gamesa 5.8 MW turbines. Their power curve is shown in Figure 3, with the black dotted lines. The cut-in speed starts at 3.5 m/s, and starts to cut out at 21 m/s, before generation stops above 26 m/s. The red line in Figure 6 shows the thrust coefficient.

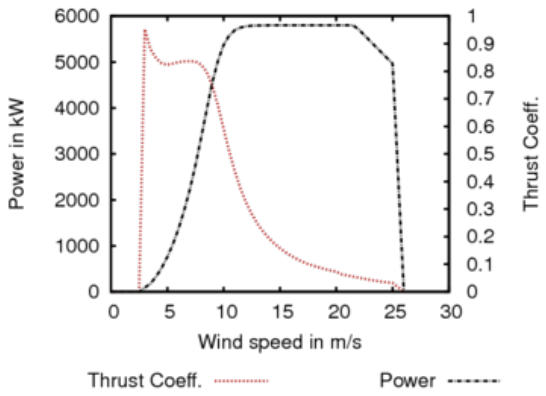

Figure 3. SG 5.8 MW power generation curve.

2.2 Columbia River Gorge

The Columbia River Gorge site of interest is a 60km x 60km subset that contains 15 wind farms. A list of the wind farm size is shown in Table 1. These wind farms are each given a conductor that is sized according to basic static ratings to have a capacity large enough to maintain the specified power production. The table also includes the conductor modeled, all of which are assumed to be ACSR and connecting from the center of the wind farm to the nearest regional transmission line. For wind farms for which data on the turbines was unavailable, a Vestas 2 MW 80m model was used. The map of the terrain elevation with the modeled wind plants is shown in Figure 4.

Table 1. Columbia River Gorge wind farms included in model.

Wind Farm	Size (MW)	Turbine	Gen Tie Conductor
Biglow Canyon	450	Vestas V82-1.65	Ruddy
Condon	50	Mitsubshi MWT600	Turkey
Dooley Mary Hill	232		Ostrich
Energizer	263		Chickadee
Golden Hills	200		Waxwing
Good Node Hills 1	96	Vestas V110-2.2	Robin
Good Node Hills 2	56	Vestas V110-2.3	Swan
Hay Canyon	101	Suzlon S88	Robin
Klondike 1	24	GE 1.5-77	Turkey
Klondike 2	76	GE 1.5-77	Sparrow
Klondike 3-1	101	GE 1.5-77	Robin
Klondike 3-2	199	GE 1.5-77	Waxwing
Star Point	100	Suzlon S88	Robin
Patu	10	GE 1.5-77	Turkey
Tuolumne	137	Siemens SWT-2.3-93	Pigeon

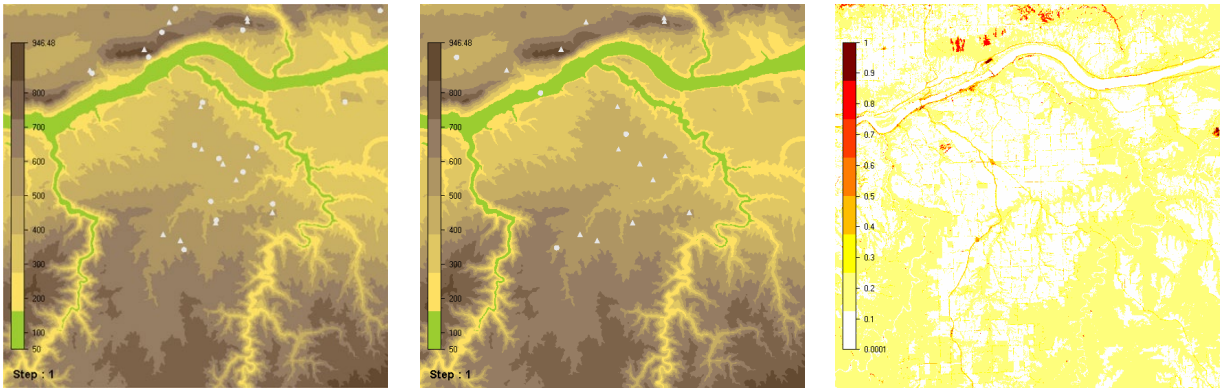

(a) (b) (c)

Figure 4. Terrain elevation of the site modeled along the Columbia River, triangles show central locations of the wind plants, (a) shows the HRRR locations with circles and (b) shows the weather station locations with circles, and (c) shows the roughness layer.

To simplify the modeling, only a single turbine was modeled for each of the representative wind plants. This may overpredict the available power from each site due to lack of wake effects. For each of the wind plants modeled, the individual turbine from Table 1 had its own specific power curve loaded into the WindSim model. The turbines' power curves are shown in Figure 5.

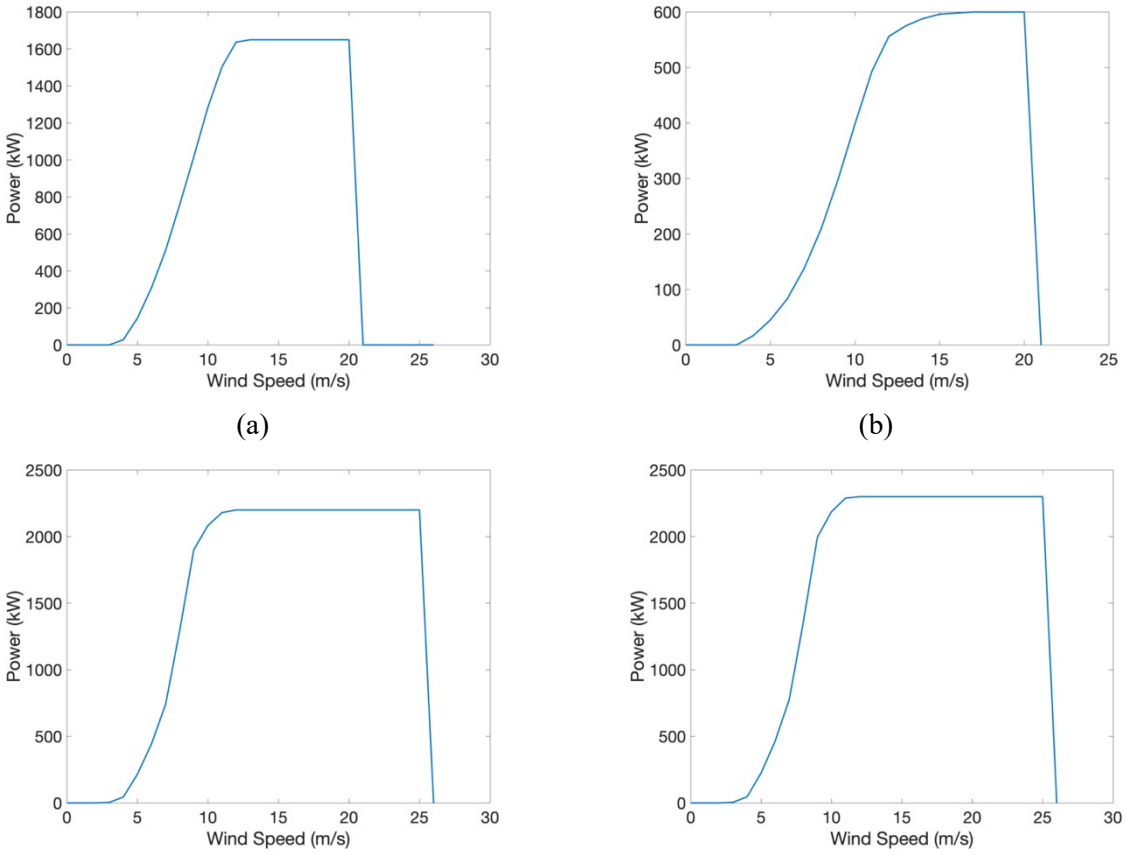

(a) (b)

(c) (d)

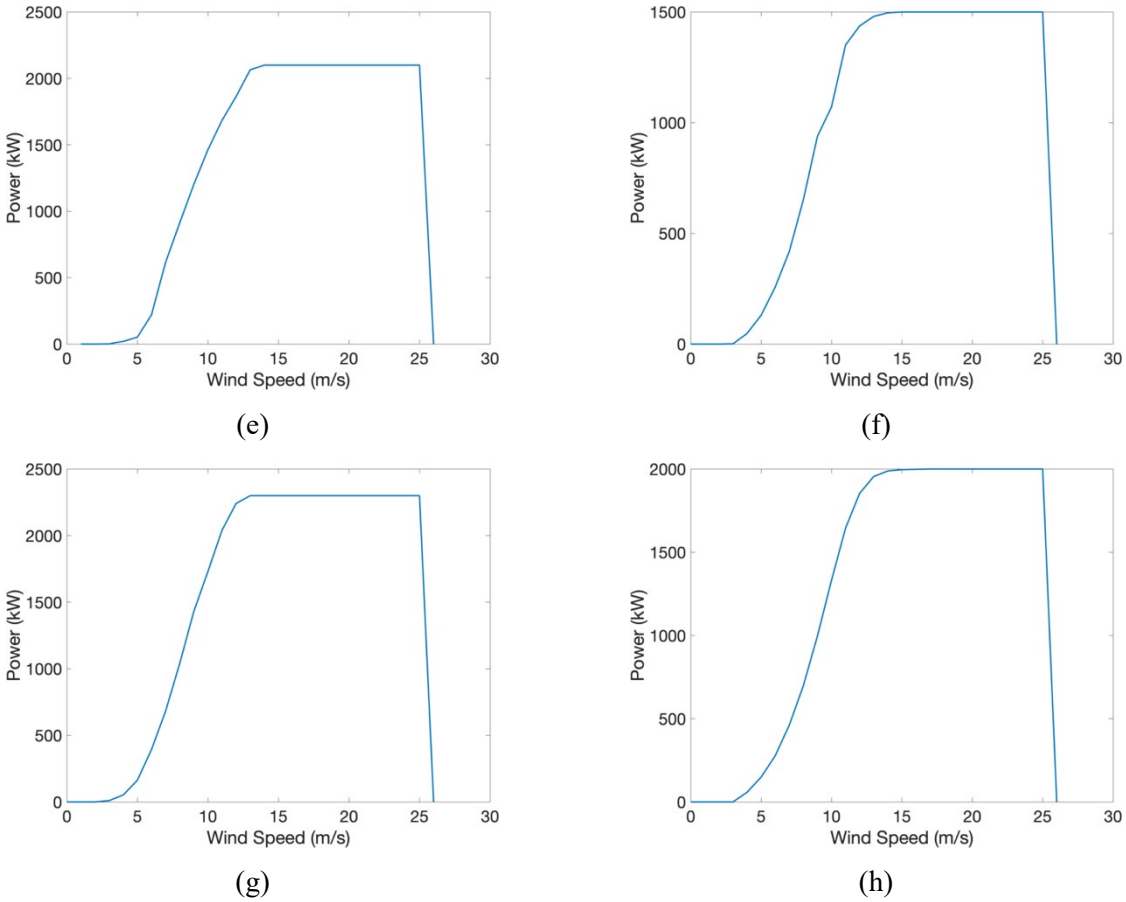

Figure 5. The turbine power curves for the modeled wind plants for (a) Vestas V82-1.65, (b) MitusbishiMWT600, (c) Vestas-V110-2.2, (d) Vestas V110-2.3, (e) Suzlon S88, (f) GE 1.5-77, (g) Siemens SWT-2.3-93 and (h) Vestas V80-2.0.

3. Methodology

3.1 Line Rating

The equations for DLR are the same used for static rating, based on a simple heat balance for a transmission line. For the weather data, the output is at 5-minute intervals. For the HRRR model data the data output is only done in hourly intervals. The heat balance equation is used to solve for the maximum current, I, to get (IEEE, 2012)

$$I = \sqrt{\frac{q_c + q_r - q_s}{R(T_c)}} \tag{1}$$

Where q_c, q_r, and q_s are the convective, radiative and solar contributions, and R is the conductor resistance as a function of the conductor temperature T_c. The radiated heat loss per unit length in units of W/m is given by

$$q_r = 17.8D\epsilon\left[\left(\frac{T_c + 273.15}{100}\right)^4 - \left(\frac{T_a + 273.15}{100}\right)^4\right] \quad (2)$$

Where ϵ is the emissivity, T_a is the ambient air temperature and D is the conductor diameter. The heat gain through solar irradiance is given by

$$q_s = \alpha Q_{se} \sin(\theta) A' \quad (3)$$

Where α is the solar absorptivity, Q_{se} is the total solar and sky radiated heat flux corrected by elevation, θ is the effective angle of incidence of the sun's rays and A' is the projected area of the conductor. The convective heat loss is calculated using one of three equations for high wind speeds, low wind speed (below 3 mph) or natural convective cooling. For high wind speed the equation is given by

$$q_{c1} = \left[1.01 + 1.35\left(\frac{DV_w\rho_f}{\mu_f}\right)^{0.52}\right] k_f K_{angle}(T_c - T_a) \quad (4)$$

For low wind speed the equation is given by

$$q_{c2} = 0.754\left(\frac{DV_w\rho_f}{\mu_f}\right)^{0.6} k_f K_{angle}(T_c - T_a) \quad (5)$$

Or for natural convection the equation is given by

$$q_{cn} = 3.645\rho_f^{0.5} D^{0.75}(T_c - T_a)^{1.25} \quad (6)$$

Where V_w is the speed of air, with fluid parameters density ρ_f, viscosity μ_f and thermal conductivity k_f calculated at the ambient temperature. And K_{angle} is the wind direction factor which can vary from about 0.3 to 1.0 based on parallel or perpendicular wind flow to the transmission line, given by

$$K_{angle} = 1.194 - \cos(\phi) + 0.194\cos(2\phi) + 0.368\sin(2\phi) \quad (7)$$

Where ϕ is the angle of incidence between the wind and the transmission line midpoint. The GLASS code developed by INL does all of these calculations for every single transmission line midpoint of interest. The minimum value among all the midpoint calculations is assumed to be the ampacity for each line.

For the gen-tie line of interest, it is assumed that the voltage is 161 kV. The maximum conductor temperature for the rating is 75 C, with an emissivity and absorptivity both equal to 0.5. For the static rating, the constant weather parameters assumed a wind speed of 2 ft/sec perpendicular to the conductor, 25 C ambient temperature, and 96 W/ft^2 solar irradiation.

Then static rating is used to determine the baseline for the conductor size that is needed for the total power of the wind farm. The dynamic line rating for each of the smaller conductors is calculated then used in Eq 8 to determine the total power carrying capacity of the gen tie line.

$$P = (3)IV \quad (8)$$

3.2 Computational Fluid Dynamics

The CFD domain for the INL site consists of 40 million computational cells, with 40-meter spatial resolution in the horizontal direction and varying spatial resolution vertically. The vertical resolution is spaced such that near the ground the resolution is in 5-meter increments to allow for accurate wind fields near the transmission lines, while above 100 meters a log scale is used up to the atmospheric boundary layer. The CFD domain for the BPA site utilizes the same vertical grid, but has 60 million cells with 60-meter spatial resolution to obtain a larger area that is modeled of 60 km by 60 km.

The steady-state standard *k*-ε RANS model is used for modelling the turbulent kinetic energy and dissipation rate. The PDEs for the solution consist of the velocity vectors, the continuity equation, and equations for the turbulent kinetic energy and turbulent dissipation rates. The equation for the velocity vectors is

$$\rho U_i \frac{\partial U_j}{\partial x_i} = \frac{\partial}{\partial x_i}\left[(\mu + \mu_t)\left(\frac{\partial U_i}{\partial x_j} + \frac{\partial U_j}{\partial x_i}\right)\right] - \frac{\partial p}{\partial x_i} \tag{9}$$

The turbulent kinetic energy, k, equation is given by

$$\frac{\partial (U_i k)}{\partial x_i} = \frac{\partial}{\partial x_i}\left[\frac{\mu_t \partial k}{\sigma_k \partial x_i}\right] + P_k - \epsilon \tag{10}$$

And the equation for the turbulent dissipate rate, , is given by

$$\frac{\partial (U_i \epsilon)}{\partial x_i} = \frac{\partial}{\partial x_i}\left[\frac{\mu_t \partial \epsilon}{\sigma_\epsilon \partial x_i}\right] + c_{\epsilon 1}\frac{\epsilon}{k}P_k - c_{\epsilon 2}\frac{\epsilon^2}{k}P_k \tag{11}$$

Where the turbulent viscosity is given by

$$\mu_t = \frac{C_\mu k^2}{\epsilon} \tag{12}$$

And the turbulent production term is given by

$$P_k = \mu_t \left(\frac{\partial U_i}{\partial x_j} + \frac{\partial U_j}{\partial x_i}\right)\frac{\partial U_i}{\partial x_j} \tag{13}$$

Where c_μ, c_{ϵ_1}, c_{ϵ_2}, σ_k, and σ_ϵ are the fixed constants for the model, with values set to 0.09, 1.55, 2.0, 1.0, and 1.3, respectively (Jones and Launder, 1972).

3.3 TREAD

INL's Transmission Route Engineering Analysis and Design [tool] (TREAD) is a tool meant for the design and routing of new transmission lines. This software takes care of much of the tedious work required to plan a new transmission line. It is capable of creating the plan for a transmission line that has been optimized for a single or multiple different values. TREAD is capable of taking an arbitrarily large amount of surface layers represented as geographical files and then using a modified version of Dijkstra's Algorithm for finding the best path based on what data is available and what has been determined to be valuable (Dijkstra, 1959).

These different shape files represent real world geometry and have associated values for various heuristic factors. These heuristic factors are such things as the cost of building on the land or adjacency to areas. The combination of these different heuristics will create a series of routes through the provided area that have been optimized for many different factors depending on what is required for the situation at hand.

The system uses the base principle behind Dijkstra's Algorithm with an infinite implied radial grid. This design choice allows for an arbitrarily large space that does not require defining rectangular resolution or boundary areas. The system is capable of running on any system that is capable of running a Java virtual machine. TREAD is also capable of interacting with different weather models in order to gather weather data about the locations that are being routed to.

This weather data is then used in conjunction with INL's General Line Ampacity State Solver to optimize the conductor for concurrent cooling or localize hot spots and then give a conductor recommendation that solves the hotspot. This process is able to happen iteratively or a single time. TREAD allows the user to graphically interact with this system and visualize, in real time, the routing that might take place. There is an arbitrary range between manual route creation and automatic route creation. Manual route creation gives the opportunity to hand design routes and test the choices with computer generated routes along the same shape files.

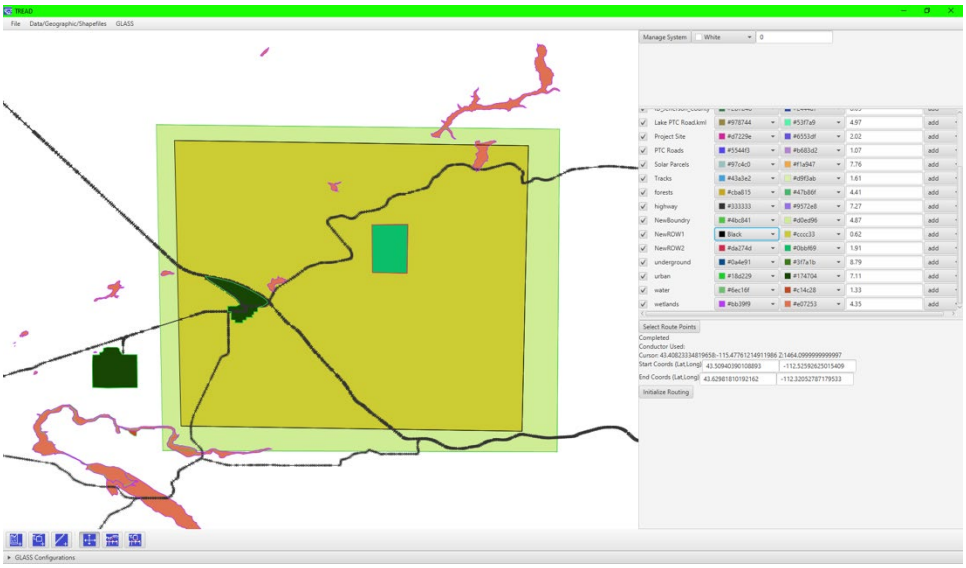

Figure 6. Example TREAD image.

4. Results

4.1 TREAD

Development of the TREAD tool for the modeling of generation tie lines was successful. The process involved loading the available data for the current transmission network and then running the TREAD application to be able to connect each center point of the wind turbines to the nearest transmission line. This process created many different transmission lines, as shown in Figure 7.

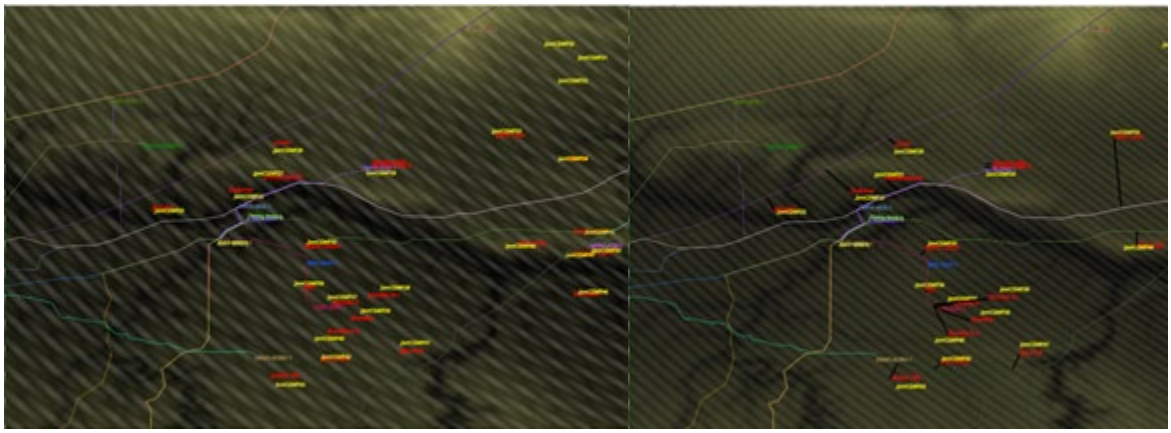

Figure 7. The (a) BPA-proposed wind generation location (yellow) and existing transmission line infrastructure. (b) The resulting gen-tie lines created with the TREAD software.

These different transmission lines were modeled taking into consideration the local geography as well as the nearest availability of forecasting points. The forecasting points used are from the National Oceanic and Atmospheric Administration HRRR model. The data from these forecasting points not only allowed for rapid, hardware-free plotting of the transmission lines, but also provides the capability to represent the points used as forecasting sources for predicting the ampacity of the transmission lines, as well as the generation capabilities of the wind plants to which they are connected.

BPA transmission line areas were used as the hypothetical basis for this study where existing lines were connected to wind-farm locations. The different wind-farm sites were connected to the main transmission networks via the computerized transmission generation. These routes conformed to the relatively flat terrain of the area travelling in a straight line to the nearest connection point available. The line routing system avoided major geographic features such as the nearby river valley.

These different lines were successfully rated via the HRRR model through expected wind conditions for the period. This has allowed for the additional rating of these lines, in some cases to be rated for an additional 25% of additional capacity over static lines. The energizer site is a 263 MW project, and the Golden Hills site is a 200 MW project. These projects must use the Partridge and Ibis aluminum-conductor steel-reinforced (ACSR) cable, rated at 283 MW and 229 MW at a voltage of 161 kV. Due to DLR, these generation stations could continue to operate and generate power under additional wind conditions for which the system was not designed. These findings have been wrapped up in a paper that is determined to go to the upcoming Conseil International des Grands Réseaux Électriques (CIGRE) grid-of-the-future conference in the winter of 2021. These results are shown in Figure 8.

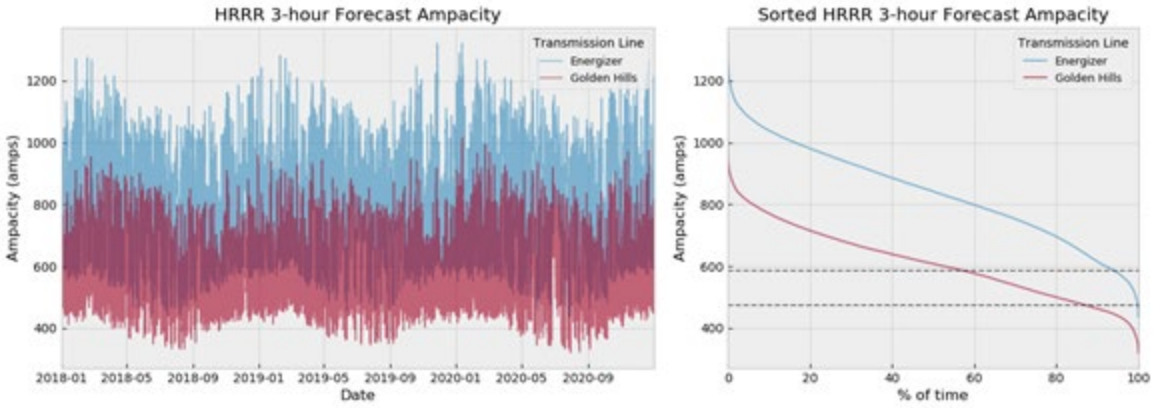

Figure 8. (a) The 3-hour HRRR forecast DLR of selected large gen-tie lines in the BPA region over a 3-year period and (b) the sorted values above the static-line rating.

The generated gen-tie lines from TREAD were then input into the WindSim CFD model to obtain the lookup tables needed to account for the local wind speed differences. With the large number of lines these had to be input into WindSim in small batches to avoid memory limitations. The set of modeled gen-tie lines for the BPA region is shown in Figure 9.

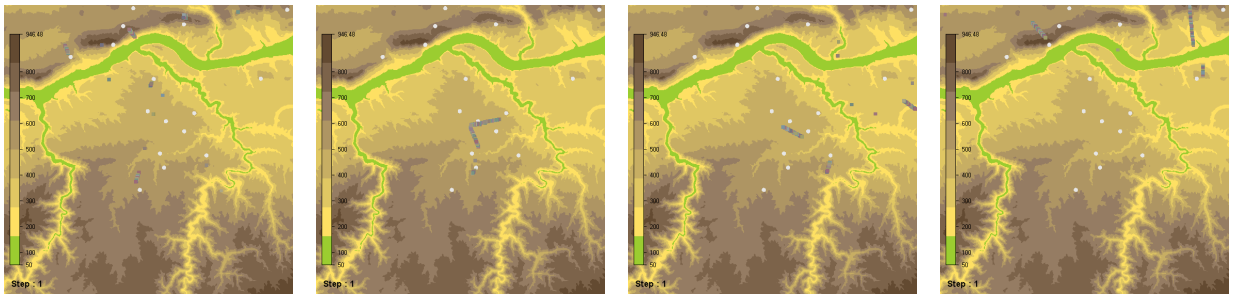

Figure 9. The set of gen-tie lines modeled in WindSim overlaid on the terrain elevation layer, the squares show the midpoint spans for each of the gen-tie lines.

The TREAD tool was also used to compare the gen-tie lines for the INL site, though the results were nearly the same as the actual gen-tie line proposed for the wind plant and were not used further on in the study. The output from the TREAD system is shown below in Figure 10. The route shown makes roughly a straight line towards the main road running through the area and then proceeds to follow this road until reaching the transmission tie point. This is an expected result for a setup like this, looking at how the area is organized will usually result in a line that the system will follow. Humans are especially good at image processing and pattern recognition, both of which is used in a routing algorithm. This usually yields a route which people would call intuitive.

The data set available to generate this route is quite small with very few depth of layers. This is one of the contributions to a highly intuitive route. The TREAD system demonstrates its value of when dealing with multiple overlapping shape files that would be tedious to look up by hand and find the value that influences the routing. With TREAD there is not theoretical limit to the number of layers that could be used and the costing function that could be applied.

In even the most complex of systems often times the routes appear very intuitive. The primary cause of this is that straight lines are always the least expensive way to route points, the routing process becomes less about finding a unique way through large obstacles but rather finding the easiest point to

route through and then creating a series of these points to wherever they need to go, this once again creates a simple and intuitive path.

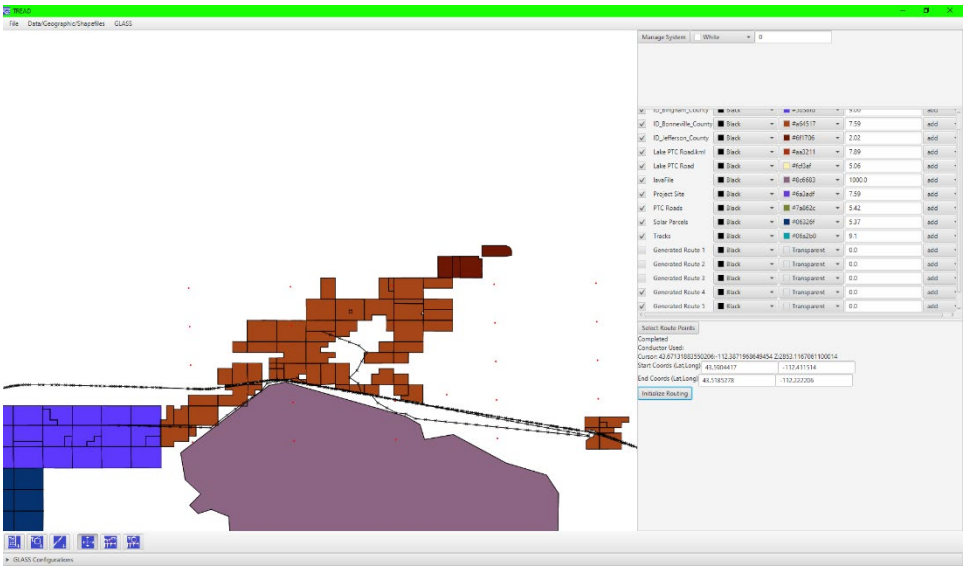

Figure 10. TREAD plots.

4.2 Weather Station Data/Computational Fluid Dynamics

Respectively, Figures 11a and 11b show distributions of wind data collected from 2018 to 2020 by the Kettle Butte weather station (latitude: 43.547, longitude: –112.326) and the nearest set of HRRR 3-hour forecasted data (latitude: 43.532, longitude: –112.322). These distributions show that near-term predictions are in agreement with observed wind conditions, having similar profiles. The most notable difference between the two distributions is that forecasts predict more wind currents traveling south than what was recorded in observational data, though the difference is minimal overall.

Figures 11c and 11d respectively show diurnal profiles of solar and temperature data collected by KET and the nearest set of HRRR 3-hour forecasted data. The yearly trend observed in the two data sets are very similar, having closely related envelopes with respect to daily maxima of solar and temperature values, though weather observations show more erratic maxima throughout the year than what is predicted in forecasts. This has a lesser impact on the DLR of the gen tie line compared to other weather quantities (e.g., wind speed or direction).

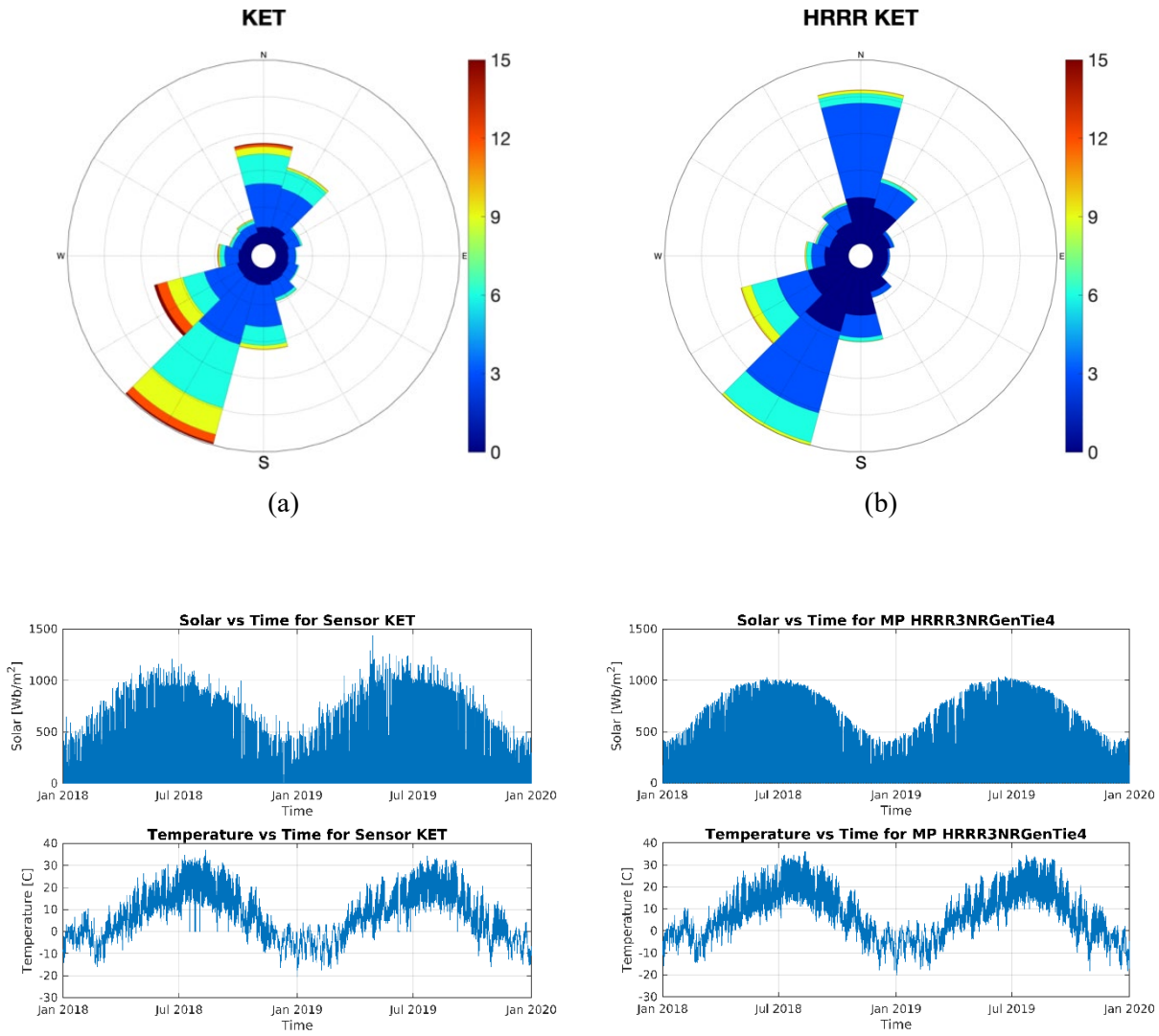

Figure 11. The Kettle Butte weather station data wind statistics (a) and diurnal profiles (b) compared to the closest HRRR model point wind statistics (b) and diurnal profiles (d).

Five statistical tests were performed to assure the integrity of the weather data used, and consequently the DLR ratings. These tests consisted of checking the entire data set for wind speeds greater than 75 m/s (test 1), wind speed changes less than 0.5 m/s/hour (test 2), subsequently constant wind direction entries with varying speed (test 3), wind speed changes greater than 20 m/s (test 4), and temperature changes greater than 8°C/hour (test 5).

Each entry in the KET data was recorded approximately every five minutes. Tests 1-5 yielded percentage discrepancies of 0.00%, 6.2%, 0.74%, 0.00%, and 0.11%, respectively. These results show good overall qualities of the data, though the outstanding figure of 6.2% for the sustained wind speeds per hour can be most likely attributed to periods of low wind currents. Tests 1-5 were also performed on the forecasted data to observe differences between observational and forecasted data, but because the forecasted data was given each hour, test 2 was neglected. These four tests yielded no percentage discrepancies which is in close agreement to tests 1, 3, 4, and 5 for the KET data set.

The rest of the data from the weather stations from the INL desert site which are close enough to the wind plant and gen-tie lines are shown in Figure 5. Two of the other sites are maintained by the Idaho Department of transportation, ITD93 and ITD95. The last site is part of the weather station network maintained by NOAA, and is located nearby MFC. The HRRR model data that is closest to each of the sites is also included in Figure 12. Generally, for this region, the HRRR model data is overpredicting the wind speed that is seen observationally over the period of measurement. The ITD93 and MFC sites both show good agreement with the wind direction of the HRRR model, but the ITD95 site shows a large change in the prevailing wind directions shifting from a SW-NE flow to more directly N-S.

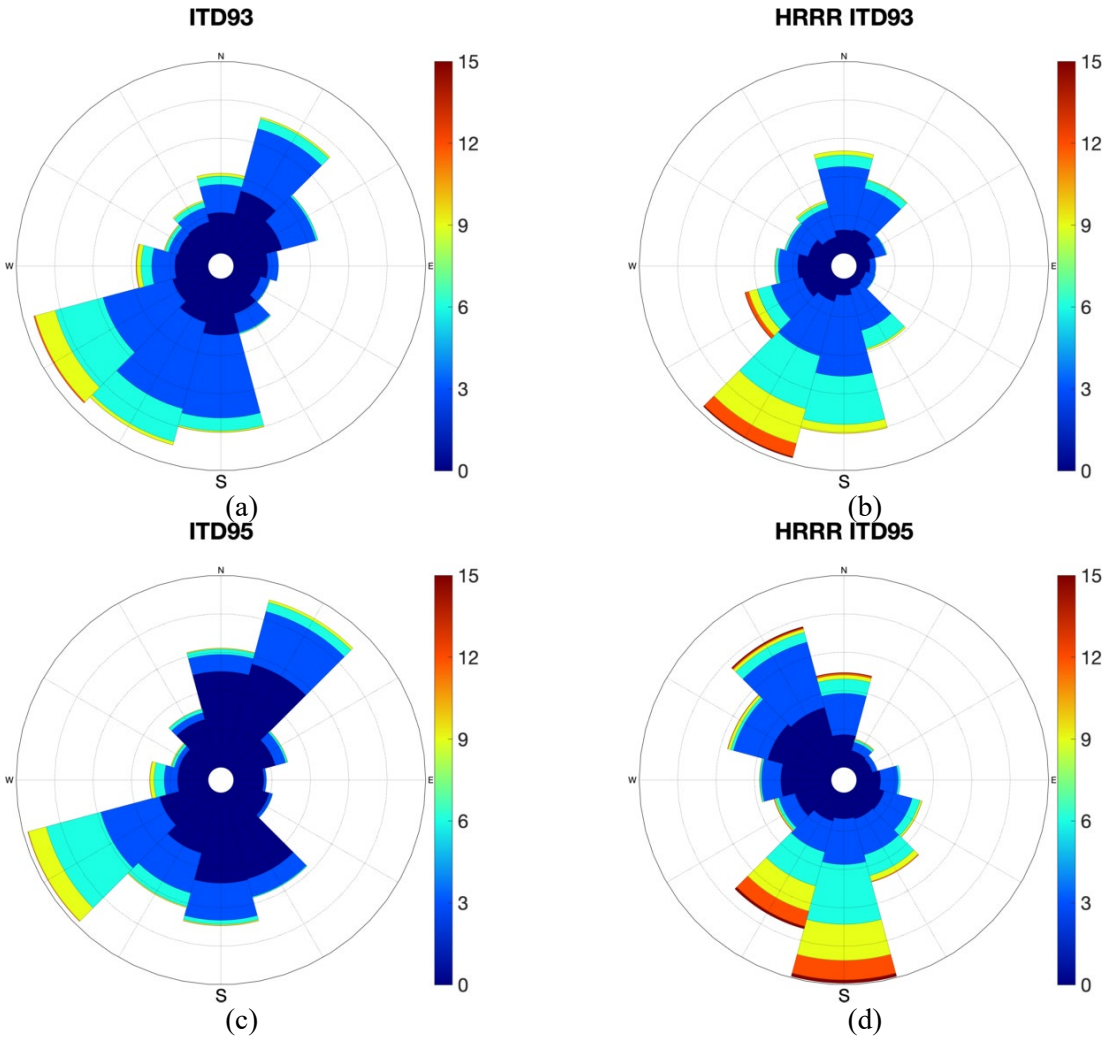

(a) (b)

(c) (d)

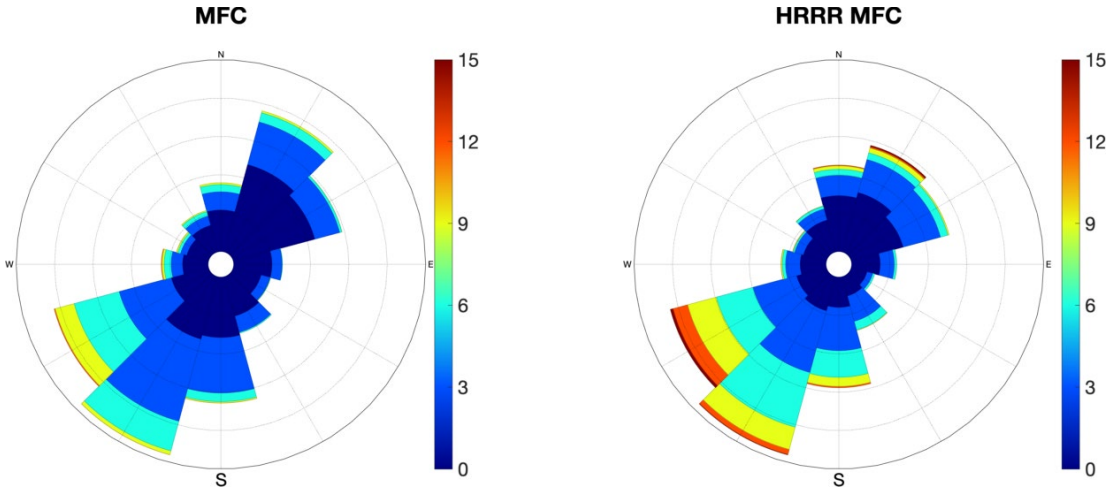

(e) (f)

Figure 12. The wind roses for the (a) ITD93 site and its (b) nearest HRRR model point, the (c) ITD95 site and its (d) nearest HRRR model point and (e) the MFC site and its (f) nearest HRRR point.

The results for the CFD wind fields are shown in Figure 13 for the domain of interest on the INL site. The data shown is for the north, east, south and west incoming wind vectors. There are eight additional sectors models at 30 degree spacing, but these are left out for brevity. The wind data is shown at two different heights, 10-meters above ground level – corresponding to the height of the transmission lines, and at 115-meters above ground level – corresponding to the hub heights of the wind turbines. The wind profile is less affected by the terrain at the higher elevations of the turbines.

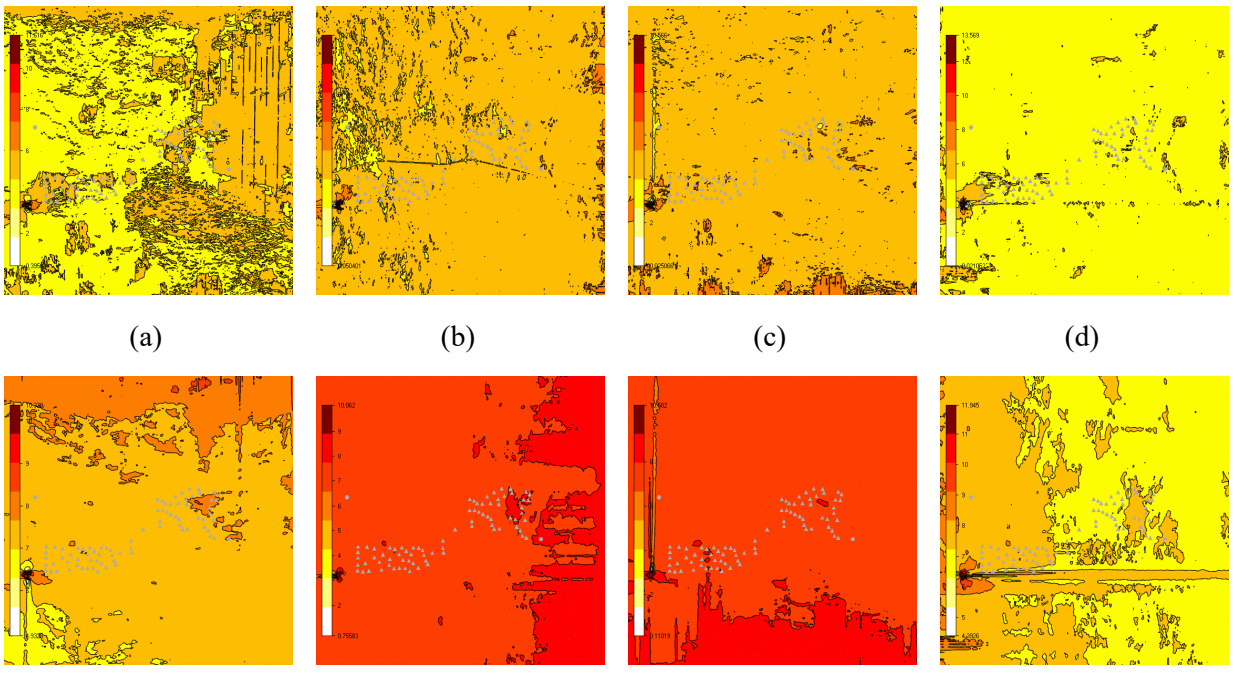

(a) (b) (c) (d)

(e) (f) (g) (h)

Figure 13. The CFD results for the heights corresponding to the gen tie lines for incoming (a) north, (b) east, (c) south and (d) west incoming wind, and the CFD results for the heights corresponding to the wind turbines for incoming (e) north, (f) east, (g) south and (h) west incoming wind.

After performing quality assurance tests on the weather stations that are within the BPA region of interest, serval weather stations in the area had to be ignored due to large gaps in the available data, long periods (i.e. months) of bad or zero speed wind speed data or other issue. Upon completing the analysis, all but three weather station sites within the domain of interest were thrown out. In this region of Oregon/Washington, the population density is extremely low, so no high-quality observations such as those typically available from the National Weather service, or local state governments such as the department of transportation were available. All three weather stations were from the citizen network, that does not have rigorous standards. The wind roses for these weather stations is shown in Figure 14. Figure 14 also shows the corresponding wind roses for the closest HRRR model data points to these weather station locations. E0859 and E2137 are near the north end of the site along the river and the direction is mostly west-to-east, this is mostly in agreement with the HRRR models, though are shifted by about 30 degrees. The D9072 is on the south end of the site further from the river gorge and shows a wider spread in directions. For this site, the HRRR model does overpredict the wind speed more than the other two. An overall comparison between the INL site and the Columbia River Gorge region shows significantly lower wind speeds in this region.

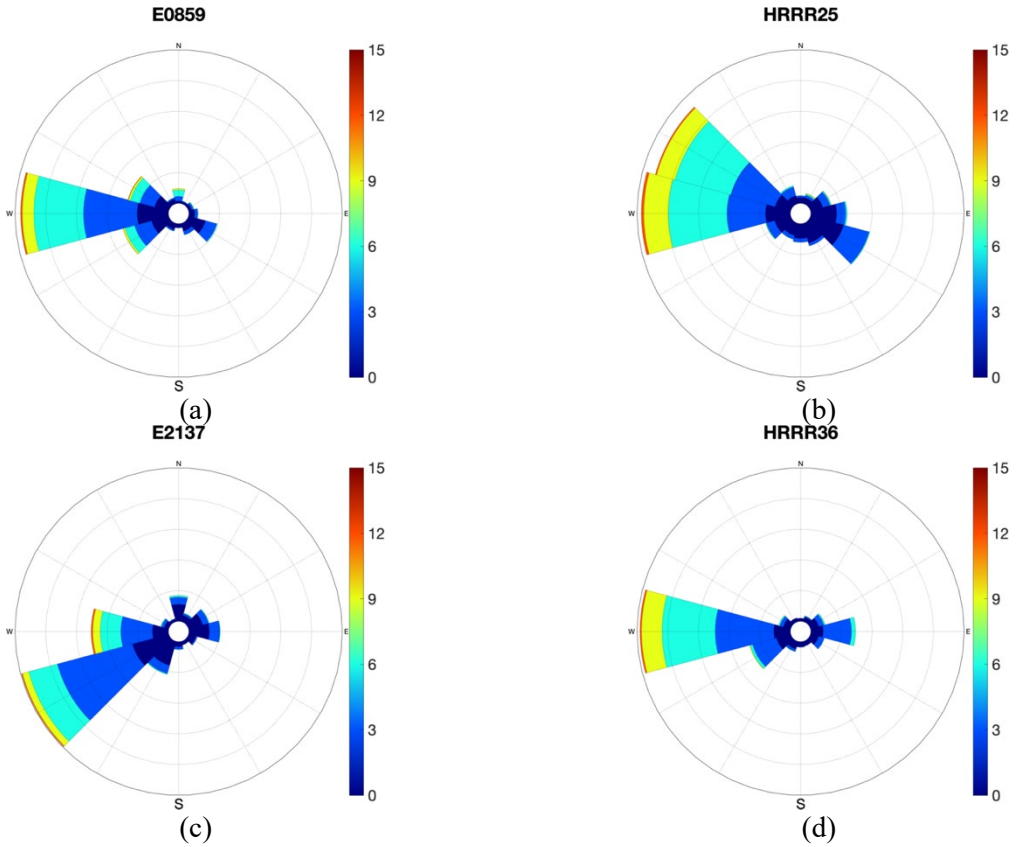

(a) (b)
(c) (d)

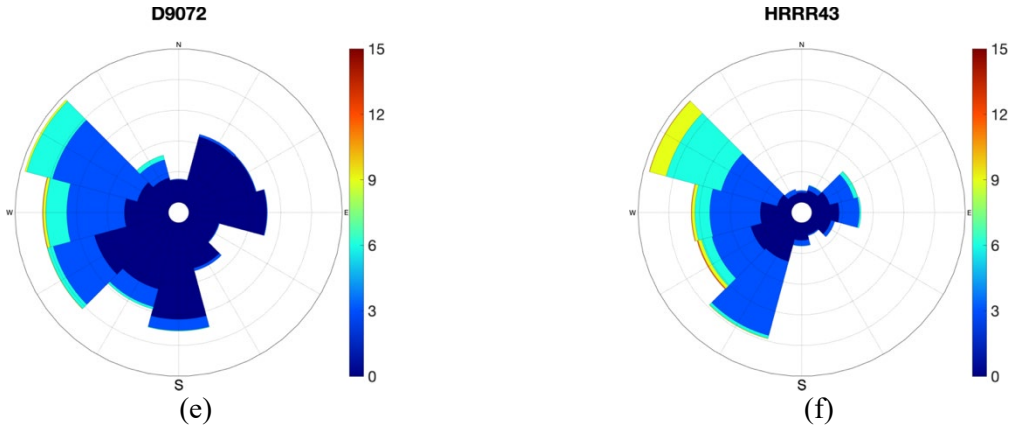

(e) (f)

Figure 14. The wind roses for the weather stations in the Columbia River Gorge (a) E0859 and (b) HRRR model point near E0859, (c) E2137 and (d) HRRR model point near E2137, (e) D9072 and (f) HRRR model point near D9072.

The results for the CFD wind fields are shown in Figure 15 for the site along the Columbia River. The data shown is for the north, east, south and west incoming wind vectors. There are eight additional sectors models at 30 degree spacing, but these are left out for brevity. The wind data is shown at two different heights, 10-meters above ground level – corresponding to the height of the transmission lines, and at 100-meters above ground level. The wind plants modeled in the BPA region vary in hub height from 65-100 meters, and those corrections are included within the WindSim CFD model. The variability in the wind speed across the BPA region is much higher than that of the INL site which is mostly flat, with the exception of the buttes. As seen in the lower set of images up at 100m, this variability remains consistent.

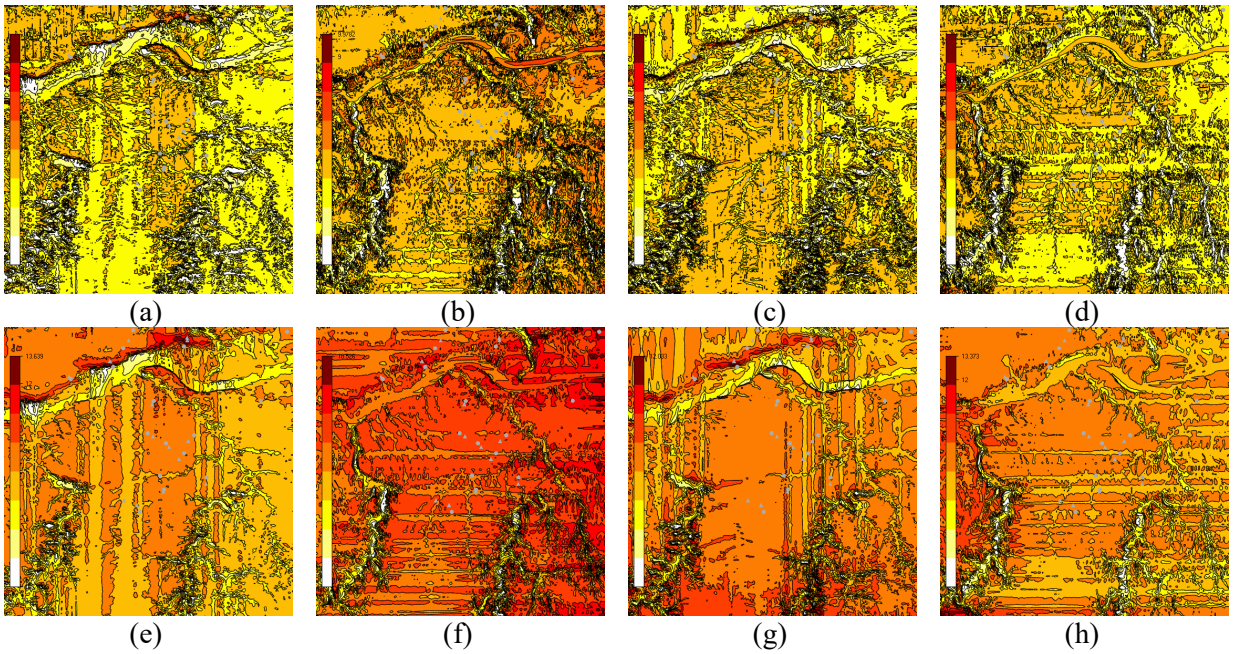

(a) (b) (c) (d)

(e) (f) (g) (h)

Figure 15. The CFD results for the heights corresponding to the gen tie lines for incoming (a) north, (b) east, (c) south and (d) west incoming wind, and the CFD results for the heights corresponding to the wind turbines for incoming (e) north, (f) east, (g) south and (h) west incoming wind for the BPA region.

4.3 Weather Data/Forecast Uncertainty

The weather data and the forecast data for regions the weather stations that were nearby the turbines of interest were directly compared to give an error in the predicted ampacity calculation between utilizing forecast and observational weather data for the region. The uncertainty for the weather stations on the INL site that are nearby the turbines are shown in Table 2. The uncertainty for the weather stations in the Columbia River Gorge region that are nearby the wind farms are shown in Table 3.

Table 2. Uncertainty of INL desert site ampacity forecasts.

Station	3-hour uncertainty	36-hour uncertainty
ITD93	13.0%	14.4%
ITD95	22.9%	25.9%
MFC	17.0%	18.8%
KET	18.7%	20.1%

Table 3. Uncertainty of Columbia River Gorge ampacity forecasts.

Station	3-hour uncertainty	36-hour uncertainty
E0859	16.5%	21.3%
E2137	15.3%	17.6%
D9072	5.7%	6.8%

4.4 Wind Farm Power Generation at INL

This power curve is used for the power generation of the turbines shown in Figure 1. They are split equally into two sites. Site 1 is in the turbines in the southwest and has a maximum generation of 225 MW. Site 1 is connected to site 2 by gen tie-line 1. Site 2 is in the north east and gen tie-line 2 carries a maximum generation of 450 MW. Figure 16 shows a week-long period of wind generation at each site and the total generation. This figure also shows the static line rating for gen tie-line 1 and 2 using the base line conductor of ACSR Partridge and Bluejay, respectively. These conductors allow for the maximum power output of the wind farm. The static capacity was determined using the static weather conditions given in Section 2.1. This results in ampacity of 475 and 1,092 amps for the lines, respectively. The lines have a voltage of 161,000 and this results in a static power rating for the gen tie-lines of 230 and 528 MW, respectively.

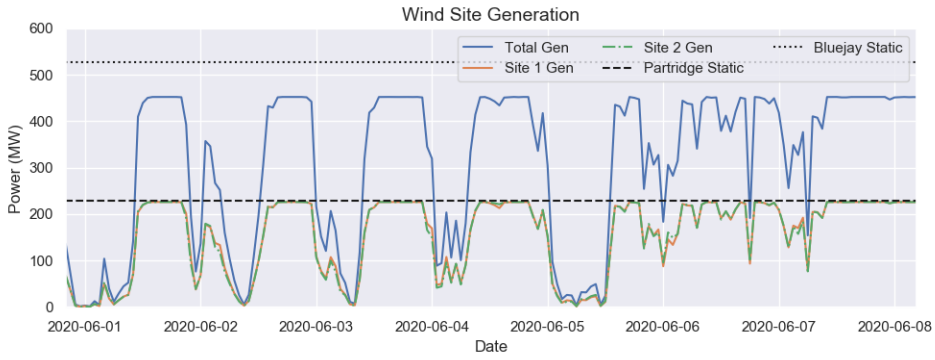

Figure 16. Wind Generation at sites 1 and 2, as well as the total generation. The static power rating of each gen tie-line is also shown.

4.5 Wind Farm Power Generation at Columbia River Gorge

For each of the wind plants modeled within the Columbia Reiver Gorge region, the power generated was calculated with both the nearest observational weather data, and the nearest HRRR model point. Each wind plant was modeled with only a single turbine associated with the central location. The wind power generation curve from each individual turbine is multiplied by the number of turbines in the wind plant to achieve the correct maximum power output. The histograms for the wind plant power generation are shown in Figure 17. Here the power generation of the observed wind speeds is shown in blue, and the forecasted wind speeds is shown overlaid in red. The difference in wind speeds between the HRRR model points and the observed model point leads to a large disparity at the tail ends of the distribution, where the observed wind speed data often has long periods of zero wind speed observed, such that the calculated power generation is also zero.

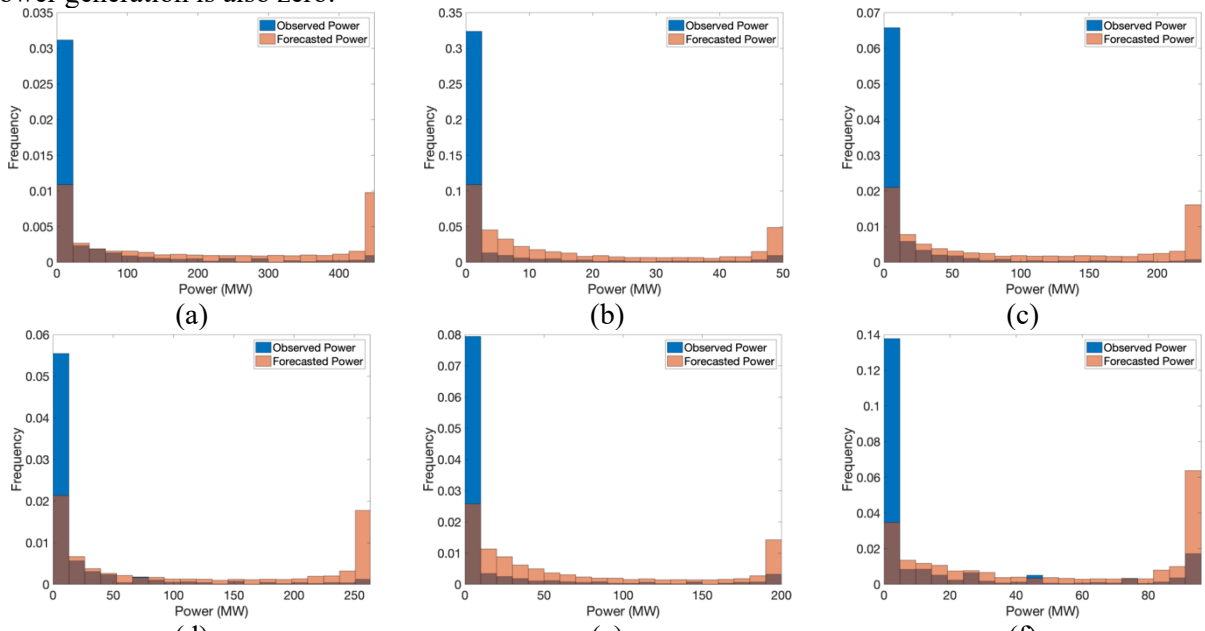

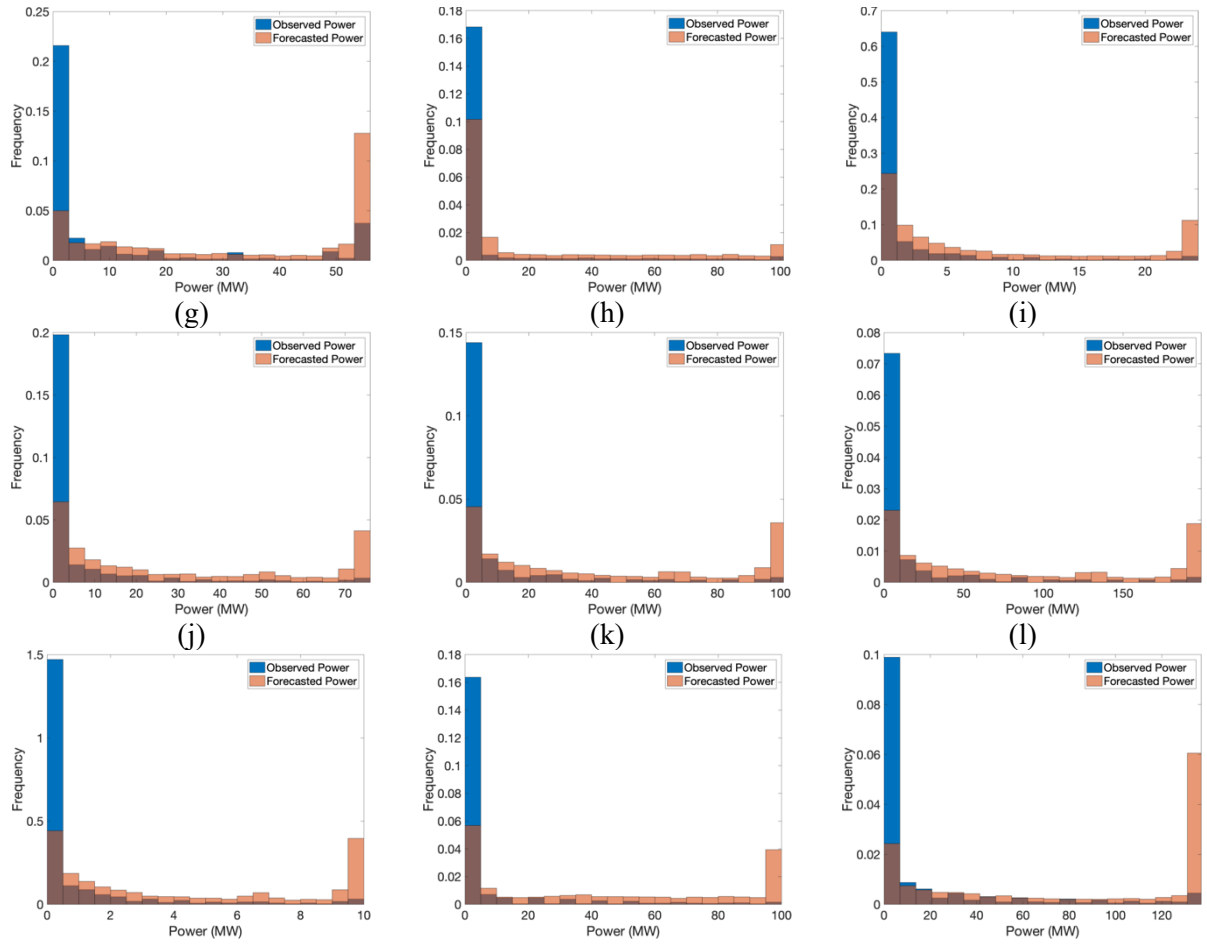

Figure 17. The raw ampacity and raw wind power generation for (a) Biglow Canyon, (b) Condon (c) Dooley Mary Hill (d) Energizer, (e) Golden Hills, (f) Good Node Hills-1, (g) Good Node Hills-2, (h) Hay Canyon, (i) Klondike-1, (j) Klondike-2 (k) Klondike 3-1 (l) Klondike 3-2, (m) Patu, (n) Star Point, (o) Tuolumne.

4.6 Dynamic Line Rating at INL Site

The dynamic line rating is calculated in ampacity. To evaluate the conductor transmission capacity in megawatts Equation 8 is used and referred to as the dynamic power capacity. The results of the dynamic power capacity of the baseline conductor Ibis in gen tie-line 1 over a week-long period is shown by the top plot in Figure 18. Here, the power flow is shown as calculated by the weather station data and the HRRR3 and HRRR36 models. The bottom plot is the dynamic power capacity error for each one of the models over the same timeframe. The error is calculated as

$$error = P_{HRRR} - P_{WS}$$

Where P_{HRRR} is the power results of the HRRR3 or HRRR36 forecast and P_{WS} is the power calculated from the weather station. Therefore, a positive value represents when the forecast model over predicts the power capacity of the line.

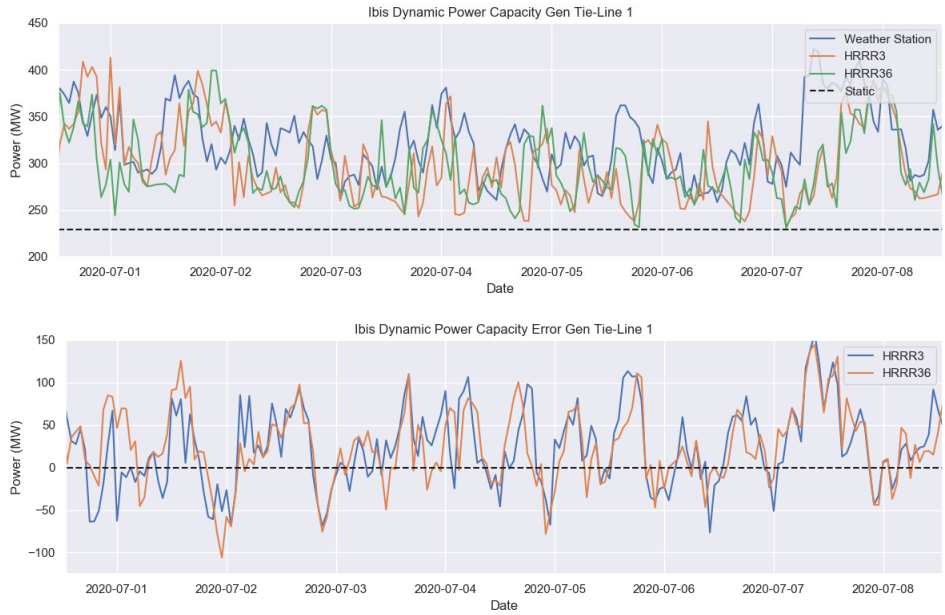

Figure 18. Dynamic power capacity (top) and error of HRRR3 and HRRR36 (bottom) over a week-long period using baseline Ibis conductor on gen tie-line 1.

Using the error of the models the root mean squared error is calculated as

$$RMSE = \sqrt{\frac{\sum_{i=1}^{N}(P_{HRRR} - P_{WS})^2}{N}}$$

where N is the number of data points. The results of the RMSE for both tie-lines are given in Table 4. Due to different capacity of different conductors the percent error is calculated as

$$\%\ error = \frac{|P_{HRRR} - P_{WS}|}{P_{WS}} * 100$$

This value is the used in the RMSE to replace the error resulting in a %RMSE, given mathematically as

$$\%RSME = \sqrt{\frac{\sum_{i=1}^{N}\left(\frac{P_{HRRR} - P_{WS}}{P_{WS}} * 100\right)^2}{N}}$$

Table 4. Dynamic power capacity RMES and %RMSE for potential conductors on each gen tie-line.

	Conductor	HRRR3		HRRR36	
		RSME	%RSME	RSME	%RSME
Gen Tie	Ibis	55.0	15.2	55.0	15.4
	Partridge	54.2	15.6	43.2	15.8

	Pigeon	30.4	16.1	30.5	16.3
Gen Tie Line 2	Bluejay	153.0	19.1	151.8	19.3
	Snowbird	145.8	19.2	144.7	19.4
	Drake	127.4	19.4	126.5	19.6
	Gull	112.1	19.6	111.3	19.8
	Ibis	82.9	20.0	82.4	20.2

4.7 Dynamic Line Rating at Columbia River Gorge

The ampacity for each of the gen-tie lines for the 15 wind plants was calculated using INL's GLASS tool. As shown in Table 2, each of the gen-tie line uses a different conductor that is sized such that it should match the maximum wind power production when a static rating is applied. However, for the Columbia Gorge region, most of these gen-tie lines are below the static ampacity for a significant amount of time. As shown previously through the wind roses, the average wind speed in the region is a bit less than that which occurs at the INL site. For each individual tie line, the ampacity is calculated and binned up then plotted against the static to show the amount of time the the capacity is above or below the static rating. The plots for this are shown for all the wind plants in Figure 19. While many of the gen tie lines show expected high additional capacities, several of these DLR-rated gen-tie lines show nearly 50% of the time under static rating.

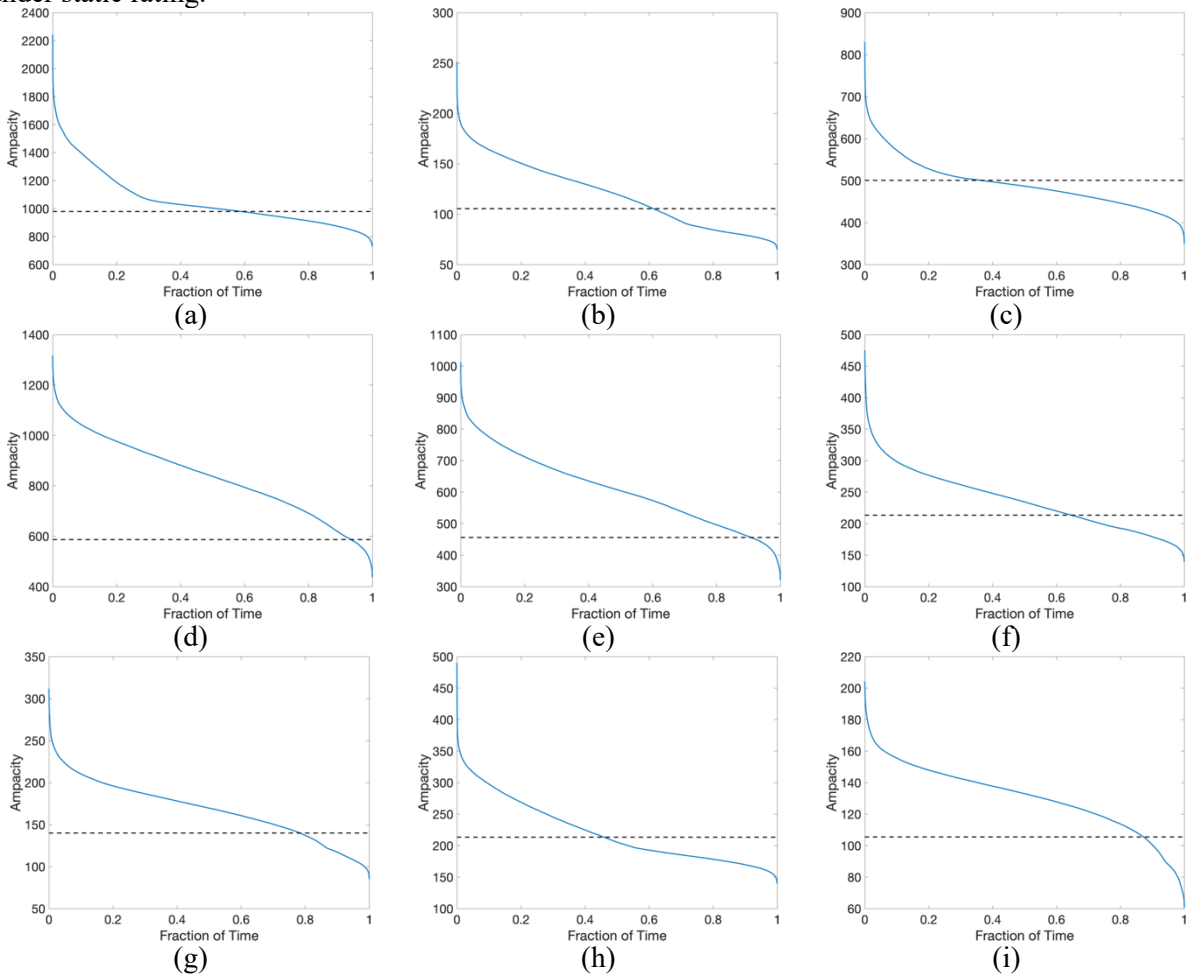

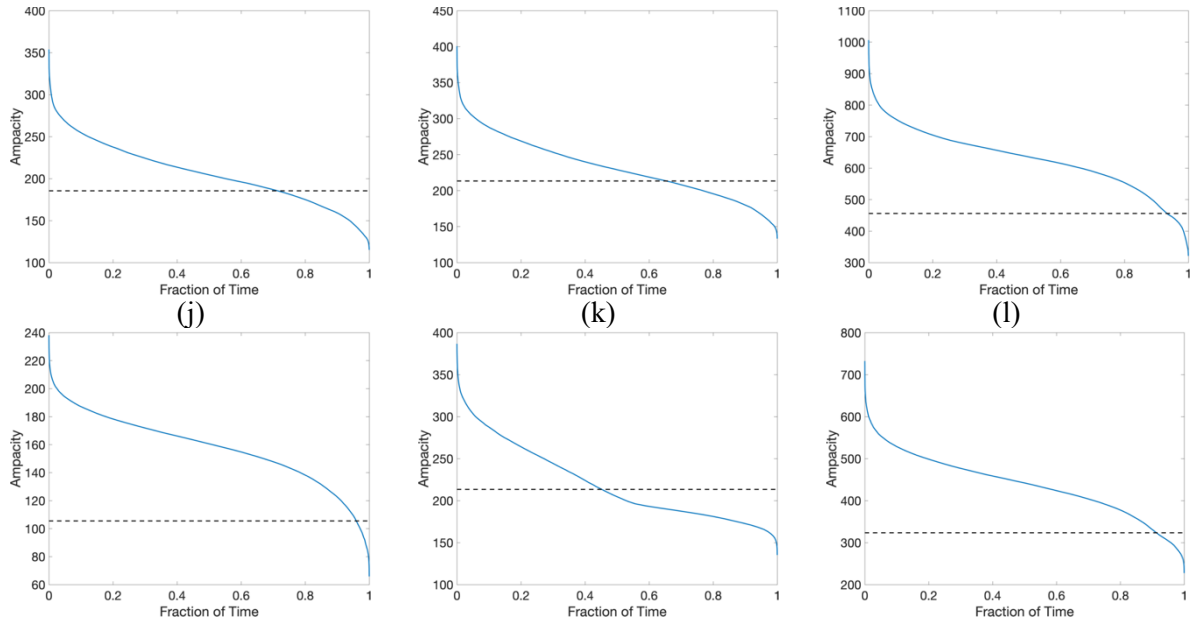

Figure 19. The binned DLR ampacity compared to the static rating for (a) Biglow Canyon, (b) Condon (c) Dooley Mary Hill (d) Energizer, (e) Golden Hills, (f) Good Node Hills-1, (g) Good Node Hills-2, (h) Hay Canyon, (i) Klondike-1, (j) Klondike-2 (k) Klondike 3-1 (l) Klondike 3-2, (m) Patu, (n) Star Point, (o) Tuolumne.

4.8 Concurrent Cooling at INL Site

The concurrent cooling effect is the analysis of how much additional power capacity is available on the gen tie-line compared to the wind generation power. A week-long period of wind generation and dynamic line rating using the baseline conductor is shown in Figure 20. Here, the concurrent cooling in the top plot is defined as the Partridge DLR – Site 1 Gen.

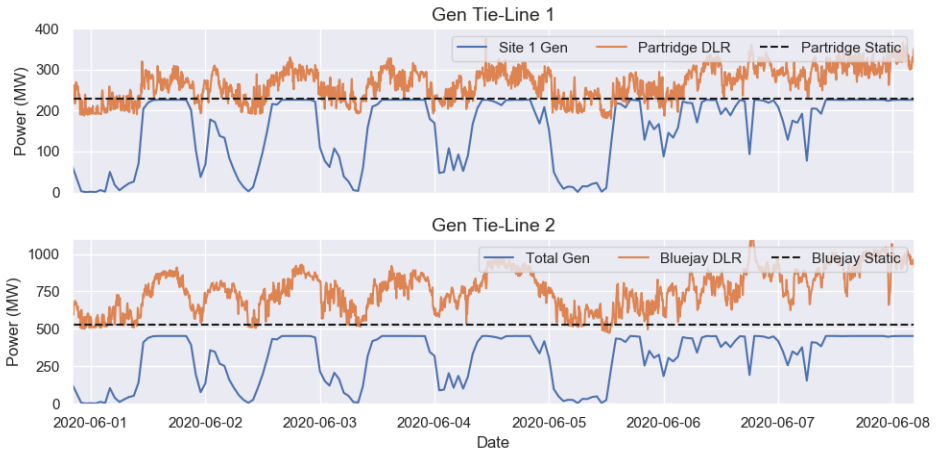

Figure 20. Concurrent Cooling of the wind generation and dynamic power capacity.

The concurrent cooling is calculated over the calendar year 2020 using the baseline conductor as well as ACSR Ibis and Pigeon for gen tie-line 1 and ACSR Snowbird, Drake, Gull, and Ibis for gen tie-line 2. The results are sorted and shown in Figure 21. Here, the percent of time and additional capacity on each line based on different conductors is clear. For example, the power capacity of a Pigeon conductor for gen

tie-line 1 is below the site 1 generation 78% of the time. Furthermore, the baseline conductor Partridge exceeds it 100% of the time and has a minimum additional capacity of 3 MW, while the Ibis conductor has a minimum additional capacity of 69 MW. The results are further detailed in Table 5.

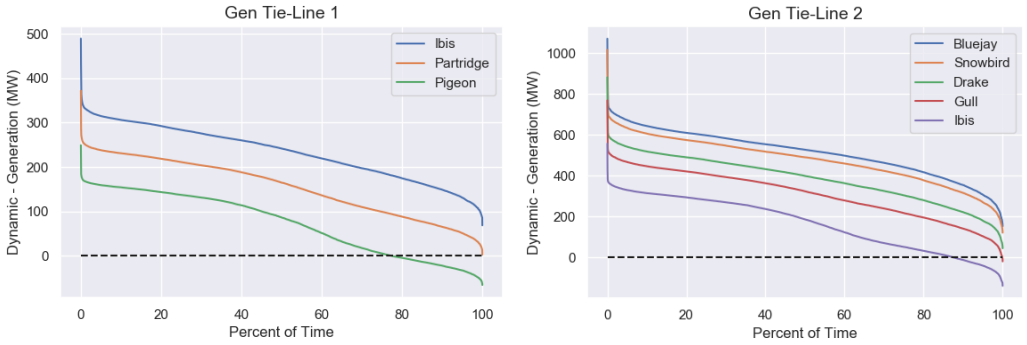

Figure 21. Access power capacity vs. percent of time using the dynamic power capacity.

Table 5. Concurrent cooling Summary.

	Conductor	Percent of Time				
		80%	90 %	95%	99%	100%
Gen Tie Line 1	Ibis	175	149	131	105	68
	Partridge	89	66	51	31	3
	Pigeon	-4	-21	-32	-49	-65
Gen Tie-Line 2	Bluejay	417	354	307	233	153
	Snowbird	377	316	270	199	122
	Drake	280	221	180	116	45
	Gull	196	141	104	48	-19
	Ibis	32	-12	-40	-83	-138

For the cost of the gen-tie line, a simple analysis can be done on the cost of the conductor itself. Online calculators (https://www.wireandcableyourway.com/acsr-aac-aaac) are available to estimate the cost of ACSR conductors on a $/length basis. The total length of gen-tie line 1 is 18253 m, and the total length of gen-tie line 2 is 19916 m. For gen-tie line 1, the approximate cost for these lines in Table 1 is then $95,220, $114,983, and $41,322 for the Ibis, Partridge and Pigeon lines. The Pigeon line could provide a conductor with minimal curtailment at a savings of $74,000. For the gen-tie line 2, the approximate costs are $262,682, $219,555, $196,685, $146,370, $103,896 for Bluejay, Snowbird, Drake, Gull and Ibis conductors. Thus, for the second gen tie with 450 MW capacity, by utilizing DLR on the ampacity, the conductor used could be a Drake instead of a Bluejay, with no generation that would need to be curtailed, for a potential savings in construction of about $65,000. If management of the real time ampacity were coupled with curtailment of the wind and possible regional capacity, further savings could be achieved through construction of a Gull conductor for curtailment less than 1% of the time or an Ibis conductor with curtailment about 10% of the time, for cost savings of about $115,000 and $160,000 for the conductor of the gen tie line.

4.9 Concurrent Cooling at BPA Wind Plants

Table includes the amount of time in the first column that each gen-tile line is above its static rating. The second column summarizes the amount of time that the gen-tie capacity calculated with the DLR rating is above the wind power generation. For lines that have low DLR compared to the static rating, if the DLR ampacity still exceeds the wind power generation, then no curtailment would be needed. Most lines are exceeding the needed capacity 90-99% of the time, only one wind plant has a line with a low capacity. It's possible that a gen-tie optimized for wind direction could exceed the value for the poorer performing gen-tie lines more often.

Table 6. Columbia River Gorge gen-tie capacities.

Wind Farm	Gen-tie ampacity over Static (%)	Gen-tie capacity over wind power generation (%)
Biglow Canyon	63.1	91.3
Condon	61.8	86.8
Dooley Mary Hill	37.8	91.5
Energizer	93.1	99.9
Golden Hills	92.4	99.9
Good Node Hills 1	65.6	95.4
Good Node Hills 2	81.2	97.2
Hay Canyon	44.3	94.3
Klondike 1	88.6	99.9
Klondike 2	72.8	99.8
Klondike 3-1	67.1	93.5
Klondike 3-2	93.6	99.9
Star Point	44.9	93.8
Patu	96.5	99.9
Tuolumne	93.7	99.9

The plots in Figure 22 shows the specifics for half of the lines. The total wind power generated is shown in red, and the total MW capacity of the DLR-rated gen tie line is shown in blue. Next to each plot of the raw data, the subtraction of this data is then binned up and plotted to show the amount of time that each of the gentile lines has additional capacity. Many of these wind plants have additional capacity that could be utilized if it were possible to install more turbines at that location without infrastructure improvements to be made to the gen-tie lines. The plots in Figure 11 show the data for the second half of the modeled gen-tie lines for the wind plants.

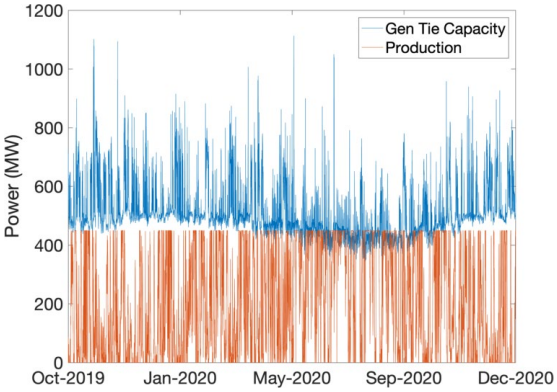
Gen Tie Capacity
Production
Power (MW)
1200
1000
800
600
400
200
0
Oct-2019
Jan-2020
May-2020
Sep-2020
Dec-2020

(a)

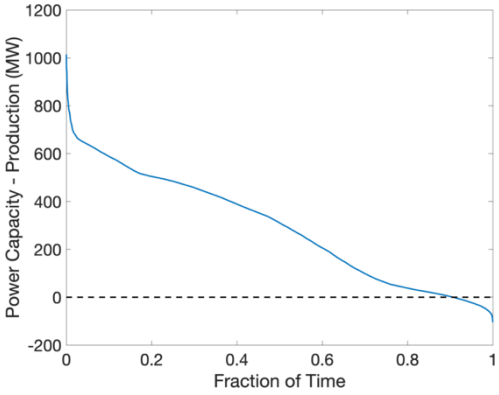
Power Capacity - Production (MW)
1200
1000
800
600
400
200
0
-200
0
0.2
0.4
0.6
0.8
1
Fraction of Time

(b)

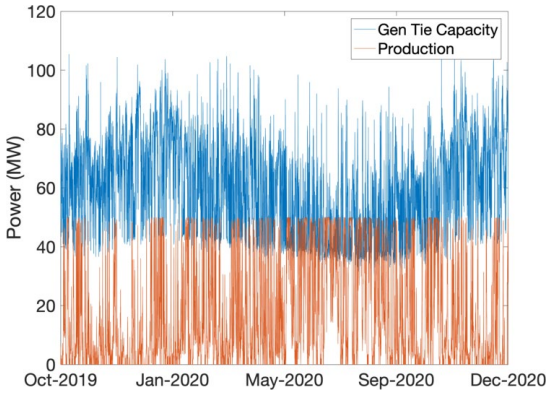
Gen Tie Capacity
Production
Power (MW)
120
100
80
60
40
20
0
Oct-2019
Jan-2020
May-2020
Sep-2020
Dec-2020

(c)

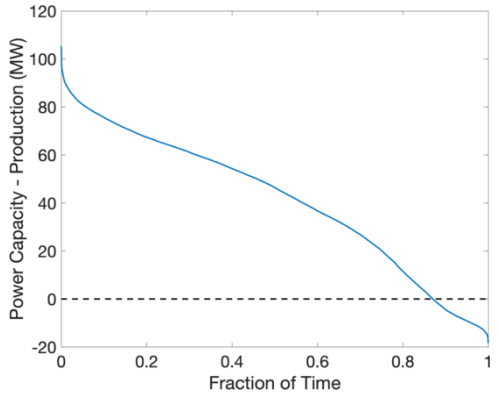
Power Capacity - Production (MW)
120
100
80
60
40
20
0
-20
0
0.2
0.4
0.6
0.8
1
Fraction of Time

(d)

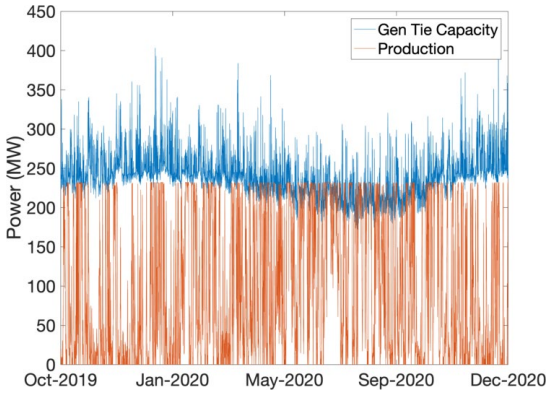
Gen Tie Capacity
Production
Power (MW)
450
400
350
300
250
200
150
100
50
0
Oct-2019
Jan-2020
May-2020
Sep-2020
Dec-2020

(e)

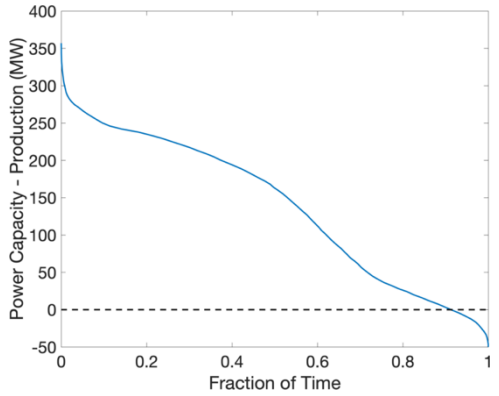
Power Capacity - Production (MW)
400
350
300
250
200
150
100
50
0
-50
0
0.2
0.4
0.6
0.8
1
Fraction of Time

(f)

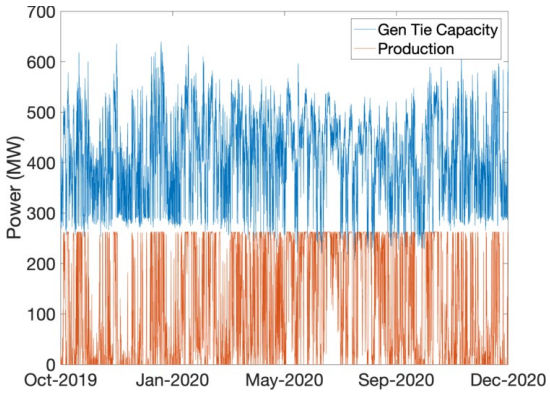
Gen Tie Capacity
Production
Power (MW)
700
600
500
400
300
200
100
0
Oct-2019
Jan-2020
May-2020
Sep-2020
Dec-2020

(g)

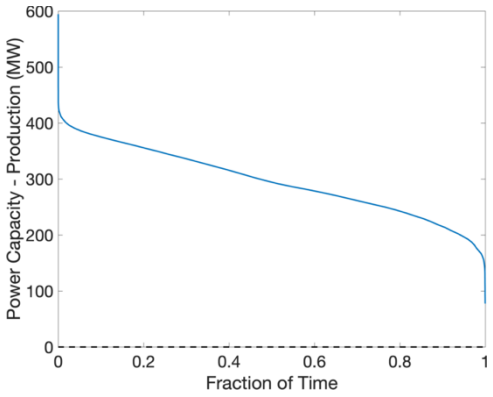
Power Capacity - Production (MW)
600
500
400
300
200
100
0
0
0.2
0.4
0.6
0.8
1
Fraction of Time

(h)

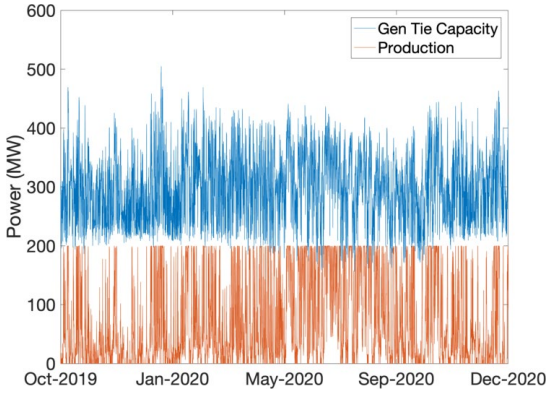
Gen Tie Capacity
Production
Power (MW)
600
500
400
300
200
100
0
Oct-2019
Jan-2020
May-2020
Sep-2020
Dec-2020

(i)

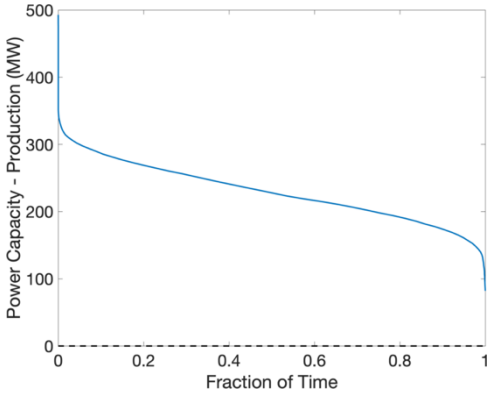
Power Capacity - Production (MW)
500
400
300
200
100
0
0
0.2
0.4
0.6
0.8
1
Fraction of Time

(j)

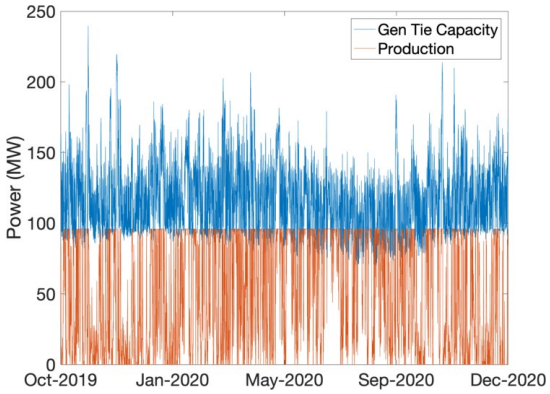
Gen Tie Capacity
Production
Power (MW)
250
200
150
100
50
0
Oct-2019
Jan-2020
May-2020
Sep-2020
Dec-2020

(k)

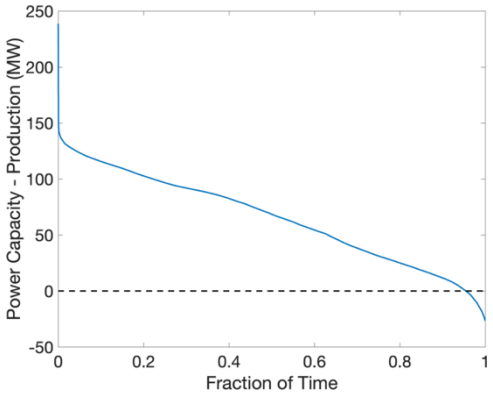
Power Capacity - Production (MW)
250
200
150
100
50
0
-50
0
0.2
0.4
0.6
0.8
1
Fraction of Time

(l)

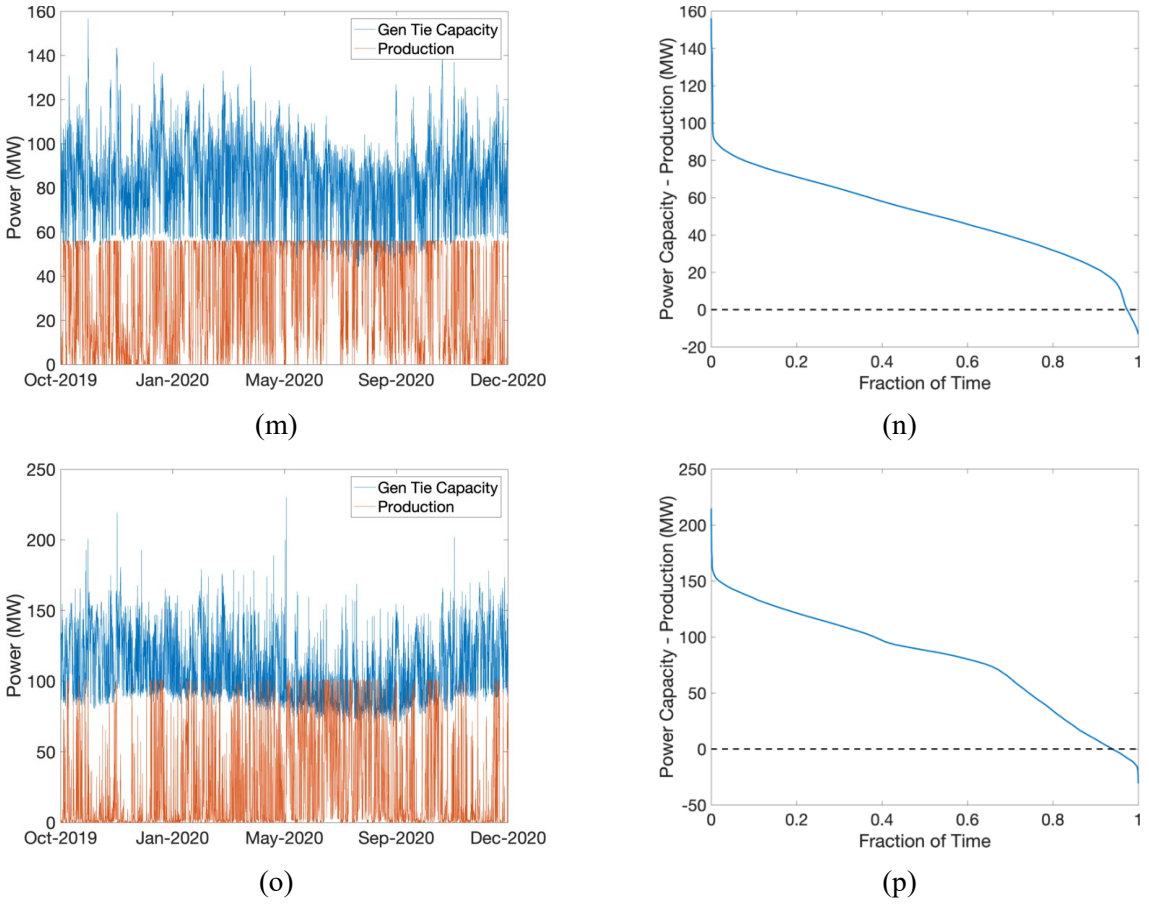

Figure 22. The raw ampacity and raw wind power generation for (a) Biglow Canyon, (c) Condon (e) Dooley Mary Hill (g) Energizer, (i) Golden Hills, (k) Good Node Hills-1, (m) Good Node Hills-2, (o) Hay Canyon. The amount of time that gen-tie line capacity is above wind power generation for (b) Biglow Canyon, (d) Condon, (f) Dooley Mary Hill (h) Energizer, (j) Golden Hills, (l) Good Node Hills-1, (n) Good Node Hills-2, (p) Hay Canyon.

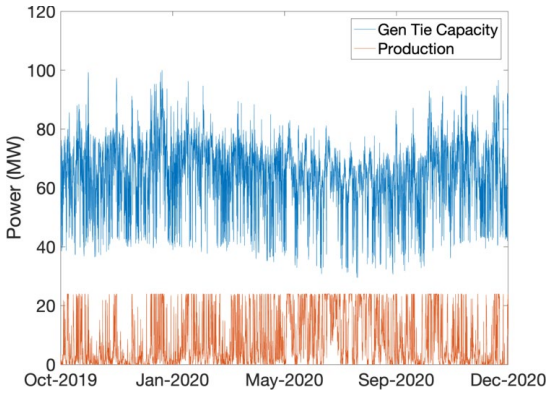
Gen Tie Capacity
Production
Power (MW)
120
100
80
60
40
20
0
Oct-2019
Jan-2020
May-2020
Sep-2020
Dec-2020

(a)

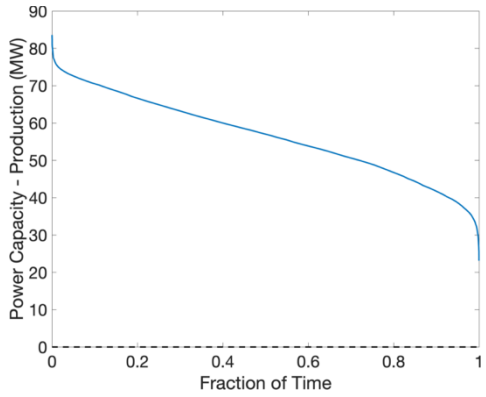
Power Capacity - Production (MW)
90
80
70
60
50
40
30
20
10
0
0
0.2
0.4
0.6
0.8
1
Fraction of Time

(b)

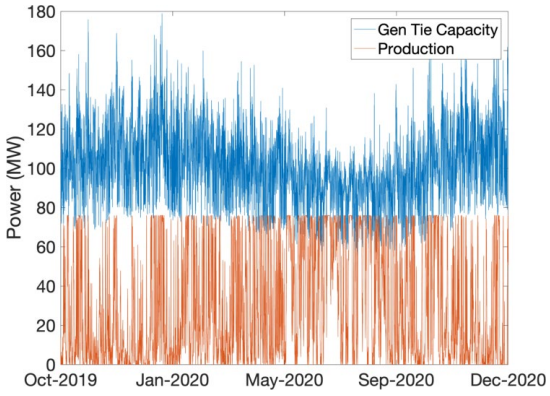
Gen Tie Capacity
Production
Power (MW)
180
160
140
120
100
80
60
40
20
0
Oct-2019
Jan-2020
May-2020
Sep-2020
Dec-2020

(c)

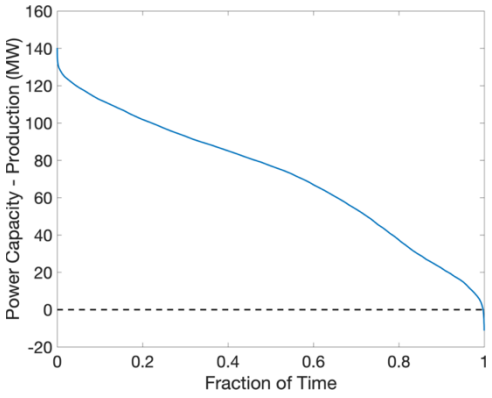
Power Capacity - Production (MW)
160
140
120
100
80
60
40
20
0
-20
0
0.2
0.4
0.6
0.8
1
Fraction of Time

(d)

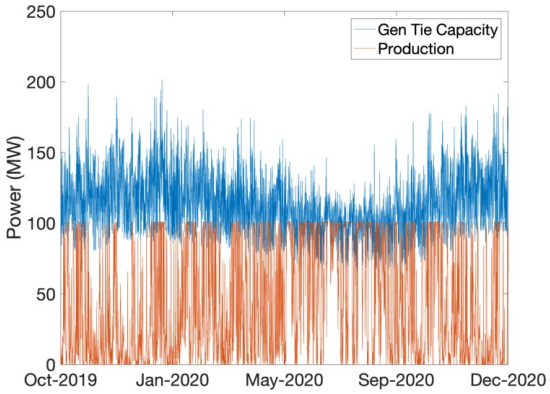
Gen Tie Capacity
Production
Power (MW)
250
200
150
100
50
0
Oct-2019
Jan-2020
May-2020
Sep-2020
Dec-2020

(e)

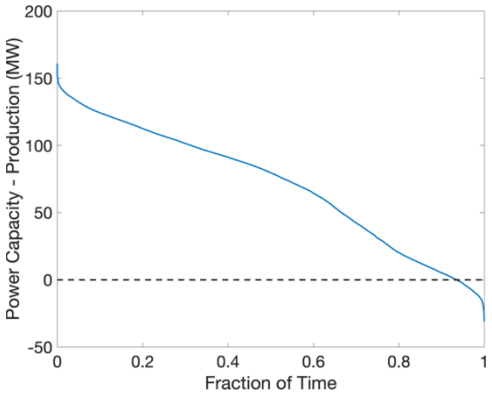
Power Capacity - Production (MW)
200
150
100
50
0
-50
0
0.2
0.4
0.6
0.8
1
Fraction of Time

(f)

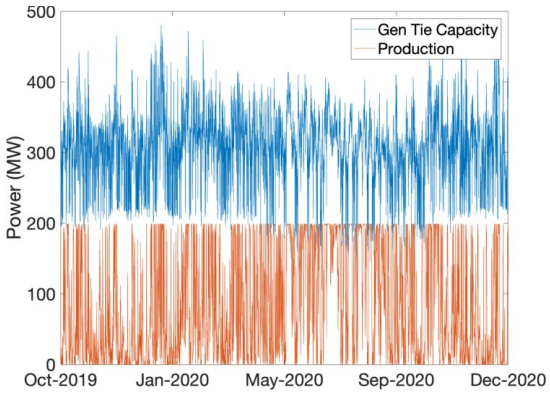
Gen Tie Capacity
Production
Power (MW)
0
100
200
300
400
500
Oct-2019
Jan-2020
May-2020
Sep-2020
Dec-2020

(g)

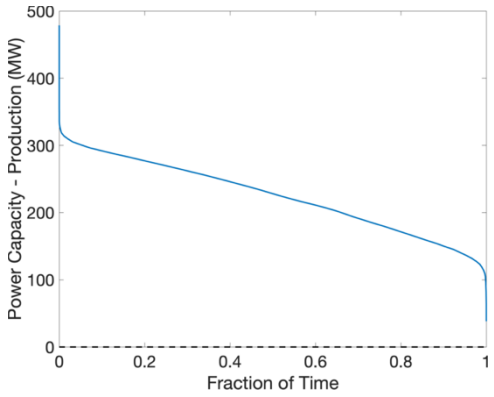
Power Capacity - Production (MW)
0
100
200
300
400
500
0
0.2
0.4
0.6
0.8
1
Fraction of Time

(h)

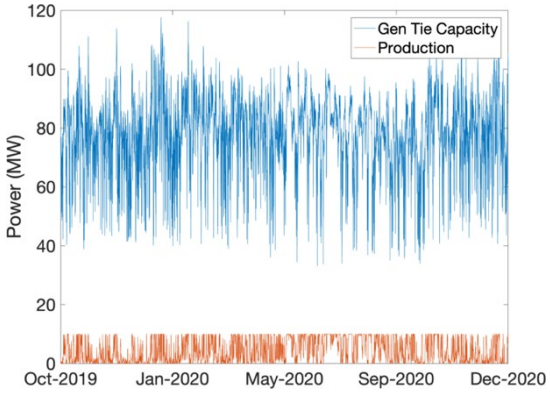
Gen Tie Capacity
Production
Power (MW)
0
20
40
60
80
100
120
Oct-2019
Jan-2020
May-2020
Sep-2020
Dec-2020

(i)

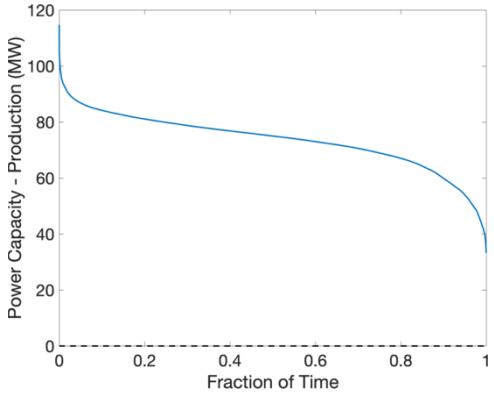
Power Capacity - Production (MW)
0
20
40
60
80
100
120
0
0.2
0.4
0.6
0.8
1
Fraction of Time

(j)

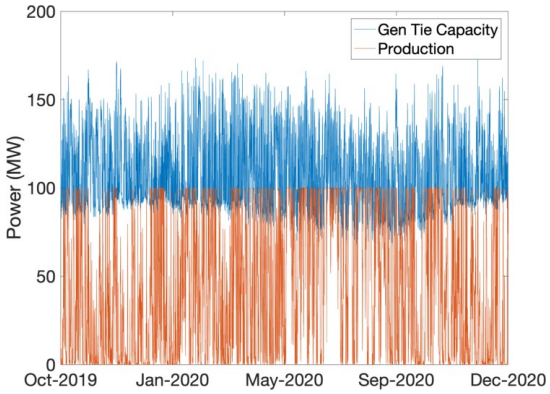
Gen Tie Capacity
Production
Power (MW)
0
50
100
150
200
Oct-2019
Jan-2020
May-2020
Sep-2020
Dec-2020

(k)

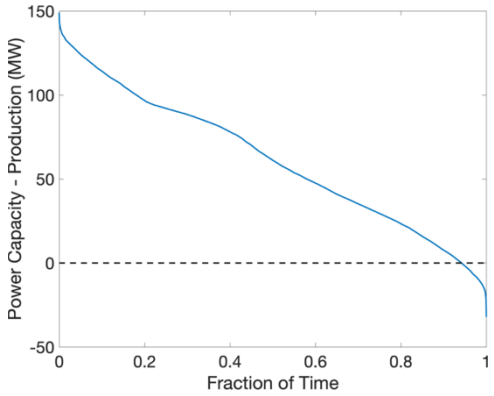
Power Capacity - Production (MW)
-50
0
50
100
150
0
0.2
0.4
0.6
0.8
1
Fraction of Time

(l)

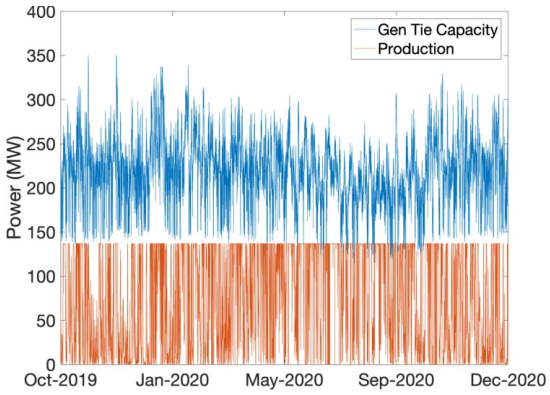

(m)

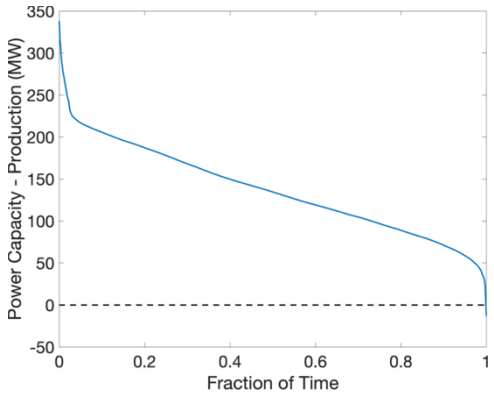

(n)

Figure 23. The raw ampacity and raw wind power generation for (a) Klondike-1, (c) Klondike-2 (e) Klondike 3-1 (g) Klondike 3-2, (i) Patu, (k) Star Point, (m) Tuolumne. The amount of time that gen-tie line capacity is above wind power generation for (b) Klondike-1, (d) Klondike-2 (f) Klondike 3-1 (h) Klondike 3-2, (j) Patu, (l) Star Point, (n) Tuolumne

5. Conclusions

A selection of wind plants across Idaho and the Columbia River Gorge were used to create of model of the wind power production coupled with dynamic line rating of gen-tie lines for forecasted and observational weather data. While the Columbia Gorge sites often showed DLR ratings far below static, which only small exceptions, these times would not coincide with times with high wind power generation, so that there should not be expected overage temperatures on the system. For both the Columbia Gorge and Idaho areas, the sites show that a statically rate gen-tie could carry additional capacity far above the rated during periods of high wind due to the concurrent cooling effects.

In both of these regions the interactions of the dynamic line rating for the regional transmission lines are also of interest. While the majority of the gen-tie lines show available capacity for the coupled wind plants, if this power capacity is not also available on the larger grid, further infrastructure improvements would be needed. The next step of this study will be to examine the regional transmission line DLR ratings in comparison with the wind power generation curves. It will also be of interest to examine the improvements on the regional transmission lines for DLR over a simple ambient adjusted rating method, which relies only on the temperature.

REFERENCES

Abboud, Alexander W., Kenneth R. Fenton, Jacob P. Lehmer, Benjamin A. Fehringer, Jake P. Gentle, Timothy R. McJunkin, Katya L. Le Blanc, Melissa A. Petty, and Matthew S. Wandishin. "Coupling computational fluid dynamics with the high resolution rapid refresh model for forecasting dynamic line ratings." *Electric Power Systems Research* 170 (2019a): 326-337.

Abboud, Alexander W., Jake P. Gentle, Timothy R. McJunkin, and Jacob P. Lehmer. "Using Computational Fluid Dynamics of Wind Simulations Coupled with Weather Data to Calculate Dynamic Line Ratings." *IEEE Transactions on Power Delivery* 35, no. 2 (2019b): 745-753.

J. Ahmad, A. Malik, L. Xia, N. Ashikin,"Vegetation encroachment monitoring for transmission lines right-of-ways: A survey, ",Electric Power Systems Research, Volume 95, 2013, pp 339-352.

B. J. L. Aznarte and N. Siebert, “Dynamic line rating using numerical weather predictions and machine learning: A case study,” IEEE Trans. Power Delivery, vol. 32, no. 1, pp. 335–343, 2017.

B. Banerjee, D. Jayaweera, S. Islam. “Risk constrained short-term scheduling with dynamic line ratings for increased penetration of wind power.” Renew Energy, 83 (2015), pp. 1139-1146.

S. G. Benjamin, S. S. Weygandt, J. M. Brown, M. Hu, C. R. Alexander, T. G. Smirnova, J. B. Olson, E. P. James, D. C. Dowell, G. A. Grell, et al., A north american hourly assimilation and model forecast cycle: The rapid refresh, Mon. Weather Rev. 144 (2016) 1669–1694.

B. P. Bhattarai, J. P. Gentle, P. Hill, T. McJunkin, K. S. Myers, A. Abboud, R. Renwick, and D. Hengst, “Trans- mission line ampacity improvements of altalink wind plant overhead tie-lines using weather-based dynamic line ratings,” in IEEE PES General Meeting, July 2017.

B. P. Bhattarai, J. P. Gentle, T. McJunkin, P. J. Hill, K. Myers, A. Abboud, and D. Hengst, “Improvement of transmission line ampacity utilization by weather-based dynamic line ratings,” IEEE Transactions on Power Delivery, 33(4), pp 1853-1863.

J. Cao, W. Du, H.F. Wang. “Weather-based optimal power flow with wind farms integration.” IEEE Trans Power Syst, 31 (4) (2016), pp. 3073-3081

CIGRE Working Group 22.12, “The thermal behaviour of overhead line conductors,” Electra, vol. 114, no. 3, pp. 107–125, 1992.

“Guide for selection of weather parameters for bare overhead conductor ratings,” CIGRE WG 22.12, Tech. Rep., 2006.

“Guide for thermal rating calculations of overhead lines,” CIGRE WG B2.43, Tech. Rep., 2014.

E.W. Dijkstra, A note on two problems in connection with graphs, Numer. Math. l (1959) 269–271.

D. Greenwood, J. Gentle, K. Myers, P. Davison, I. West, J. Bush, G. Ingram, and M. Troffaes, “A comparison of real-time thermal rating systems in the U.S. and the U.K.” IEEE Trans. Power Delivery, vol. 29, no. 4, pp. 1849– 1858, August 2014.

IEA (2021), Renewable Energy Market Update 2021, IEA, Paris https://www.iea.org/reports/renewable-energy-market-update-2021

“Overhead electrical conductors calculation methods for stranded bare conductors,” IEC Standard TR 1597, Tech. Rep., 1985.

“Standard for calculating current-temperature relationship of bare overhead line conductors,” IEEE Standard 738, Tech. Rep., 2012.

IEEE PES WG Subcommittee 15.11, “Real-time over- head transmission line monitoring for dynamic rating,” IEEE Transactions on Power Delivery, vol. 31, no. 3, 2016.

W. Jones and B. Launder, “The prediction of laminarization with a two-equation model of turbulence,” International journal of heat and mass transfer, vol. 15, no. 2, pp. 301–314, 1972.

Southwire Company, Product Database and Specifications, https://www.southwire.com/wire-cable/bare-aluminum-overhead-transmission-distribution/c/c-bare-aluminum-overhead

T. Smith, S. Benjamin, J. Brown, S. Weygandt, T. Smirnova, B. Schwartz, Convection forecasts from the hourly updated, 3-km high resolution rapid refresh (hrrr) model., in: 24th Conference on Severe Local Storms, Savanah, GA, 2008.

S. Talpur, C.J. Wallnerstrom, C. Flood, P. Hilber. “Implementation of dynamic line rating in a sub-transmission system for wind power integration.” Smart Grid Renew Energy, 6 (8) (2015), pp. 233-249

I. Toren and E. L. Petersen, European Wind Atlas. Risø National Laboratory, 1989.

“Dynamic line rating systems for transmission lines: American recovery and reinvestment act of 2009,” U.S. Department of Energy, Tech. Rep., 2014.

“Smart grid system report,” U.S. Department of Energy, Tech. Rep., 2010.

S. Uski-Joutsenvuo and R. Pasonen, “Maximizing power line transmission capability by employing dynamic line ratings technical survey and applicability in finland, vtt- r-01604-13,” Tech. Rep., 2013.

https://www.wireandcableyourway.com/acsr-aac-aaac